Compositional Mechanisms in Steam-Assisted Gravity Drainage and Expanding-Solvent Steam-Assisted Gravity Drainage With Consideration of Water Solubility in Oil

Arun Venkat Venkatramani, University of Alberta, and **Ryosuke Okuno,** The University of Texas at Austin

Summary

Experimental data have shown that the solubility of water in the oleic (L) phase (x_{wL}) can be significant at elevated temperatures. However, x_{wL} was not properly considered in prior studies of steam-assisted gravity drainage (SAGD) and expanding-solvent (ES)-SAGD. The main objective of this research is to present a detailed study of compositional mechanisms in SAGD and ES-SAGD simulation by considering x_{wL}.

The phase-behavior models used in this research are carefully created on the basis of experimental studies presented in the literature. Mechanistic simulation studies are then conducted for SAGD and ES-SAGD. Coinjectants used in ES-SAGD simulations range from propane through n-decane.

Results show that x_{wL} enhances bitumen production in both SAGD and ES-SAGD, mainly because x_{wL} results in reduction of L-phase viscosity. The enhancement is more significant when the chamber-edge temperature is higher, because x_{wL} increases with temperature. The enhancement of bitumen production observed in the case studies is 7.66% for SAGD, 4.08% for n-C_6-SAGD, and 4.85% for n-C_8-SAGD for a fixed period of operation at 35 bar. It is important to consider x_{wL} in SAGD and ES-SAGD simulations, because the performance of ES-SAGD relative to SAGD tends to be overestimated without considering x_{wL}.

A guideline is presented to leverage x_{wL} to improve bitumen production in ES-SAGD. As discussed in our prior research, solvent becomes effective in diluting bitumen and reducing the steam requirement only when it sufficiently accumulates near the chamber edge. New results show that water can act as a diluting agent until solvent sufficiently accumulates near the chamber edge.

Introduction

SAGD is currently the most widely used method for in-situ bitumen recovery (Keshavarz et al. 2014, 2015). In SAGD, steam is injected into a bitumen reservoir through a horizontal well. The injected steam forms a steam chamber, and condenses at the chamber edge, where it releases the latent heat. The heated bitumen and condensed hot water drain to another horizontal well, which is approximately 5 m below and parallel to the injection well.

The practicality of SAGD mainly comes from the high temperature sensitivity of the viscosity of bitumen. For example, experimental measurements for an Athabasca bitumen show that its viscosity is reduced by over three orders of magnitude as the temperature is increased from the initial reservoir temperature of approximately 285 K to 393 K (Mehrotra and Svrcek 1986). Despite its wide usage, the high energy and environmental costs associated with SAGD have led to the search for alternative processes (Keshavarz et al. 2014, 2015). One such alternative is the ES-SAGD process, wherein a small amount of solvent is coinjected with steam. A review on ES-SAGD is given by Keshavarz et al. (2015).

The rate at which the steam chamber propagates in SAGD and ES-SAGD depends on the extent of the improvement of the mobility of the oleic (L) phase at and beyond the chamber edge. For a given reservoir, reduction of the L-phase viscosity is largely governed by the interplay between the phase behavior of water/hydrocarbon mixtures and fluid flow, as briefly presented next (Al-Bahlani and Babadagli 2009; Amani et al. 2013a, 2013b; Keshavarz et al. 2014, 2015).

In general, there exist three phases [L, vapor (V), and aqueous (W)] within the steam chamber, whereas two phases (L and W) coexist beyond the chamber edge. Thus, the transition from three-phase (L-V-W) to two-phase (L-W) coexistence determines thermodynamic properties along the chamber edge, such as temperature, phase compositions, and phase kinematic viscosities at a given operating pressure.

Coinjection of solvent with steam can result in chamber-edge temperatures that are substantially lower than that for steam-only injection (Keshavarz et al. 2014, 2015; Khaledi et al. 2015). The chamber-edge temperature tends to decrease as the solvent accumulated near the chamber edge becomes more volatile (Keshavarz et al. 2015; Khaledi et al. 2015). The effectiveness of ES-SAGD to enhance the L-phase mobility for a given solvent at a specified operating pressure is contingent upon three aspects: (i) accumulation of solvent in the vicinity of the chamber edge; (ii) transition from L-V-W to L-W coexistence at the chamber edge; and (iii) the extent of reduction in the L-phase viscosity beyond the chamber edge, which is affected by temperature and the dilution capability of the solvent.

However, there is potentially an additional compositional mechanism that occurs at the operating temperatures of SAGD and ES-SAGD, which is often disregarded in conventional reservoir-simulation practice (Luo and Barrufet 2005). It is the dissolution of water in the L phase.

Experimental investigations on the phase behavior of water-containing mixtures of hydrocarbons including reservoir oils indicate that water can act as a diluting agent for heavy oil and bitumen. The data indicate three aspects. First, the solubility of water in the L phase (x_{wL}) can be significant at elevated temperatures (Griswold and Kasch 1942; Reamer et al. 1944; Kobayashi and Katz 1953; Skripka 1979; Tsonopoulos and Wilson 1983; Heidman et al. 1985; Glandt and Chapman 1995; Economou et al. 1997; Shinta and Firoozabadi 1997; Tsonopoulos 1999; Maczynski et al. 2005; Shaw et al. 2005, 2006a, 2006b; Amani et al. 2013a, 2013b). For example, Amani et al. (2013b) measured that x_{wL} was 54 mol% at 550 K for a mixture of water and an Athabasca bitumen. Second, the affinity of water to hydrocarbons is higher for aromatics and naphthenes in comparison with paraffins (Griswold and Kasch 1942; Tsonopoulos and Wilson 1983;

This paper (SPE 180737) was accepted for presentation at the SPE Canada Heavy Oil Technical Conference, Calgary, 7–9 June 2016, and revised for publication. Original manuscript received for review 6 March 2016. Revised manuscript received for review 8 July 2016. Paper peer approved 1 August 2016.

Heidman et al. 1985; Economou et al. 1997; Tsonopoulos 1999). Third, the dissolution of water in the L phase results in the reduction of its viscosity (Glandt and Chapman 1995). A detailed review of the phase behavior of water/hydrocarbon mixtures can be found in Venkatramani and Okuno (2015).

Luo and Barrufet (2005) used a compositional thermal simulator to show that oil recovery with steam injection was calculated to be more efficient if x_{wL} was considered. This was primarily because the water dissolution made the L-phase viscosity lower in their simulation. However, their simulation cases were presented only for relatively light oils of 20 and 35 ° API (specific gravities of 0.934 and 0.850, respectively). The significance of x_{wL} in the context of bitumen recovery with SAGD and ES-SAGD is an unsolved question in the literature. This is an important engineering question considering the high aromaticity of the L phase and high operating temperatures in these processes (Amani et al. 2013a, 2013b), which will result in high x_{wL}.

The existence of this gap in the current literature is likely an outcome of the underlying uncertainties in fluid models used in reservoir simulation. The uncertainties are the result of both the paucity of available experimental data for fluid properties and shortcomings of existing frameworks to model them (Venkatramani and Okuno 2015).

Venkatramani and Okuno (2015) presented a new framework to reliably model the multiphase compositional behavior of water-containing mixtures of reservoir oils by use of the Peng-Robinson equation of state (EOS) (PR EOS) with van der Waals' mixing rules (Peng and Robinson 1976; Robinson and Peng 1978). The framework of Venkatramani and Okuno (2015) is particularly suited for application in reservoir-engineering studies for several reasons.

First, it does not require any change in the widely used formulation on the basis of the traditional PR EOS with van der Waals' mixing rules. Second, the framework has been developed on the basis of experimental evidence. Experimental measurements indicate that three-phase curves of water/n-alkane binaries exhibit an asymptotic limit near the vapor-pressure curve of water, and that water exhibits greater affinity toward aromatics and naphthenes compared with n-alkanes. No explicit assumptions regarding the configuration of intermolecular networks have been made. This is in contrast to some recent modeling approaches such as those of Oliveira et al. (2007) and Zirrahi et al. (2015), who used complex semiempirical fluid models. Experimental evidence on the nature of intermolecular interactions in the L phase of water/hydrocarbon mixtures at elevated temperatures has not been published, to the best of our knowledge. Third, the framework offers flexibility in terms of its ability to handle the multiphase compositional behavior of different types of water/hydrocarbon systems, such as water/n-alkane mixtures and water-containing reservoir oils, which also contain aromatics and naphthenes.

The compositions of the nonaqueous phases (i.e., vapor and oleic) are accurately predicted with the framework developed by Venkatramani and Okuno (2015). A shortcoming of this method, however, is that the concentration of hydrocarbons in the W phase (x_{hcW}) is underestimated by several orders of magnitude. This underprediction is of little significance in reservoir studies focusing on mechanisms in bitumen recovery in view of the low solubility of bitumen and hydrocarbon solvents in the W phase (<0.01 mol%) even at elevated temperatures.

SAGD is the benchmark against which ES-SAGD is evaluated as an alternative. Because of the differences in the recovery mechanisms underlying SAGD and ES-SAGD, the relative performance of ES-SAGD to SAGD may be affected by how x_{wL} affects each of these processes. In this paper, therefore, the optimal application strategy is revisited considering x_{wL}, in view of its potential significance.

This paper is concerned with two important questions. The first question pertains to the significance of x_{wL} in SAGD and ES-SAGD in terms of its effect on important process variables—bitumen production rate, steam requirement, and solvent selection. The influence of operating conditions and fluid-modeling schemes on the effect of x_{wL} on bitumen production is also examined. The second question pertains to if and how x_{wL} can be used to enhance bitumen-recovery efficiency at the scale of a single well pair used in field scenarios. These questions are answered by application of the characterization framework developed by Venkatramani and Okuno (2015) in numerical thermal compositional reservoir simulations. The bitumen and solvents under consideration are an Athabasca bitumen and single-component normal alkanes, respectively.

The next section presents a mechanistic examination of SAGD and ES-SAGD including the effect of x_{wL} on bitumen recovery. In the Injection Strategy for ES-SAGD With Consideration of x_{wL} section, the results of the investigation conducted in the previous section will be used to develop an application strategy for ES-SAGD for efficient recovery of bitumen through the usage of x_{wL} as an additional compositional mechanism.

Mechanistic Study of SAGD and ES-SAGD With Consideration of x_{wL}

This section consists of three subsections. The Reservoir Model subsection and the Fluid Model subsection present the specifications of the reservoir model and the fluid model used in numerical simulations, respectively. The subsection Analysis of Simulation Results gives an analysis of the numerical simulations.

Reservoir Model. Reservoir flow simulations are performed with the STARS simulator of Computer Modeling Group (CMG 2011). The reservoir models considered are homogeneous. The initial reservoir temperature and pressure are 286.15 K and 15 bar, respectively. The initial saturation of water in the reservoir is 0.25, with the remainder being "live" Athabasca bitumen. Live bitumen considered in this research is a mixture of 1 mol% methane (C_1) and 99 mol% dead Athabasca bitumen; this corresponds to a gas–oil ratio (GOR) of 0.44 m^3/m^3. The residual saturation of oil is assumed to be 0.13. The relative permeability model used is independent of temperature. Heat losses to over- and underburden are considered in the simulations. However, other effects, such as physical dispersion, capillary pressures, and asphaltene precipitation, have not been considered.

The production well is 3 m above the base of the model, and the injection well is 4 m above the producer. The temperature of the injected stream is equivalent to the saturation temperature of water at the operating pressure. The quality of steam used is 90%. The production well is subject to the minimum bottomhole-pressure (BHP) constraint of 15 bar, which is the initial reservoir pressure. The reservoir is subject to an initial heating period of 6 months with steam during which there is no production.

Only one-half of the steam chamber is simulated in this section. The reservoir model in these cases is 70 m × 37.5 m × 20 m in the x-, y-, and z-direction, respectively; the scale of this model is identical to that used by Keshavarz et al. (2014). The original bitumen in place at stock-tank conditions is 11 591 m^3. This model is discretized into $70 \times 1 \times 20$ gridblocks in the x-, y-, and z-direction, respectively; the y-coordinate in this model represents the direction along the horizontal wells. The injection and production wells are in the left boundary of the reservoir model. The production well is subject to the maximum liquid flow-rate constraint of 200 m^3/d at surface conditions and a maximum steam flow rate of 1 m^3/d. A summary of the reservoir model is presented in **Table 1.**

Fluid Model. This section presents details of the compositional model with the PR EOS, L-phase viscosity model, and L-phase density model used for the numerical simulations. To determine the significance of water dissolution on bitumen recovery, two cases are defined: the base case, in which x_{wL} is neglected, and the water-dissolution case, in which x_{wL} is considered. For both cases, the dissolution of hydrocarbons in the W phase (x_{hcW}) is disregarded. This assumption is considered reasonable in view of low values for x_{hcW} (<1 mol%) indicated by experimental measurements (e.g., Heidemann 1974).

Property	Value
Porosity	33%
Horizontal permeability	4,000 md
Vertical permeability	3,000 md
Initial reservoir pressure at the depth of 500 m	15 bar
Initial reservoir temperature	286.15 K
Initial oil saturation	0.75
Initial water saturation	0.25
Three-phase relative permeability model (CMG 2011)	Stone's Model II
Formation compressibility	1.8E-05 1/kPa
Rock heat capacity (Keshavarz et al. 2014)	2600 kJ/m^3 °C
Rock thermal conductivity (Keshavarz et al. 2014)	660 kJ/m d °C
Over-/underburden heat capacity (Keshavarz et al. 2014)	2600 kJ/m^3 °C
Over-/underburden thermal conductivity (Keshavarz et al. 2014)	660 kJ/m d °C
Bitumen thermal conductivity	11.5 kJ/m d °C
Gas thermal conductivity	2.89 kJ/m d °C
Producer bottomhole pressure (minimum)	15 bar
Steam quality	0.9

Table 1—Summary of the reservoir model used for the SAGD and ES-SAGD simulation case studies.

The molecular weight of the Athabasca bitumen used is 530.00 g/mol. The dead bitumen has been characterized as a single pseudocomponent (C_D) with the characterization method of Kumar and Okuno (2015).

In this work, simulations for SAGD use three components: water, C_1, and C_D. Those for ES-SAGD use four components: water, C_1, C_D, and a solvent component. The solvents used for ES-SAGD in this study are *n*-alkanes; the lightest and heaviest *n*-alkanes under consideration are propane (C_3) and *n*-decane (*n*-C_{10}), respectively. Component-specific critical constants (T_C, P_C) and acentric factor (ω) are presented in **Table 2.**

The compositional behavior of water/solvent/Athabasca-bitumen mixtures is modeled with the PR EOS with the van der Waals mixing rules. The binary-interaction parameter (BIP) for C_D with *n*-alkanes has been obtained from Kumar (2016).

The BIP for water with *n*-alkanes is calculated with the correlation developed by Venkatramani and Okuno (2015) on the basis of the measured three-phase curves (*L-V-W*) of water/*n*-alkane binaries by Brunner (1990). The correlation is given as

$$\mathrm{BIP} = \mathrm{C}_1[1 + \exp(\mathrm{C}_2 - \mathrm{C}_3\mathrm{MW})]^{-1/\mathrm{C}_4}, \quad \ldots\ldots\ldots\ldots \quad (1)$$

where $\mathrm{C}_1 = 0.24200$, $\mathrm{C}_2 = 65.90912$, $\mathrm{C}_3 = 0.18959$, and $\mathrm{C}_4 = -56.81257$.

The BIP for water with C_D is expected to be lower than that for an *n*-alkane with a similar molecular weight (MW), because Athabasca bitumen contains aromatics and the affinity of water toward aromatics is greater than that for *n*-alkanes (Tsonopoulos and Wilson 1983; Heidman et al. 1985; Economou et al. 1997; Tsonopoulos 1999). As described in Venkatramani and Okuno

Component	T_C (K)	P_C (bar)	ω	MW (g/mol)
C_1	190.5611	45.9908	0.0157	16.0427
C_3	369.8278	42.4807	0.1543	44.0961
n-C_4	425.1222	37.9605	0.2014	58.1228
n-C_5	469.7000	33.7009	0.2511	72.1495
n-C_6	507.6000	30.2507	0.3010	86.1762
n-C_7	540.2000	27.4005	0.3505	100.2029
n-C_8	568.7000	24.9245	0.3980	114.2296
n-C_9	594.6000	22.9002	0.4459	128.2563
n-C_{10}	617.7000	21.1000	0.4898	142.2830
C_D	847.1700	10.6381	1.0406	530.0000
Water	647.0960	220.6400	0.3433	18.0100

Table 2—Component-specific critical constants (T_C, P_C), acentric factor (ω), and molecular weight (MW). The values of T_C, P_C, and ω for *n*-alkanes were obtained from Venkatramani and Okuno (2015). The dead bitumen was characterized as a single pseudocomponent (C_D) by the perturbation from *n*-alkanes (*PnA*) method (Kumar and Okuno 2015); this was conducted on the basis of phase equilibrium and density measurements made for methane-saturated bitumen. The pertinent experimental data were obtained from Kariznovi (2013) and Nourozieh (2013). A detailed description of the characterization method can be found in Kumar (2016).

	C_1	C_3	n-C_4	n-C_5	n-C_6	n-C_7	n-C_8	n-C_9	n-C_{10}	C_D	Water
C_1	0.000	0.000	0.000	0.000	0.000	0.000	0.000	0.000	0.000	0.000	0.732
C_3	0.000	0.000	0.000	0.000	0.000	0.000	0.000	0.000	0.000	0.067	0.666
n-C_4	0.000	0.000	0.000	0.000	0.000	0.000	0.000	0.000	0.000	0.075	0.636
n-C_5	0.000	0.000	0.000	0.000	0.000	0.000	0.000	0.000	0.000	0.081	0.607
n-C_6	0.000	0.000	0.000	0.000	0.000	0.000	0.000	0.000	0.000	0.088	0.579
n-C_7	0.000	0.000	0.000	0.000	0.000	0.000	0.000	0.000	0.000	0.094	0.553
n-C_8	0.000	0.000	0.000	0.000	0.000	0.000	0.000	0.000	0.000	0.098	0.527
n-C_9	0.000	0.000	0.000	0.000	0.000	0.000	0.000	0.000	0.000	0.102	0.503
n-C_{10}	0.000	0.000	0.000	0.000	0.000	0.000	0.000	0.000	0.000	0.105	0.480
C_D	0.000	0.067	0.075	0.081	0.088	0.094	0.098	0.102	0.105	0.000	0.169
Water	0.732	0.666	0.636	0.607	0.579	0.553	0.527	0.503	0.480	0.169	0.000

Table 3—BIP matrix for water/solvent/Athabasca bitumen. Kumar (2016) presented a correlation for the BIP for Athabasca bitumen with n-alkane solvents in terms of component-specific critical volumes. It was developed on the basis of phase-equilibrium measurements performed by Kariznovi (2013) and Nourozieh (2013) for C_3/bitumen and n-C_4/bitumen in the vapor-liquid and liquid-liquid regions. The BIPs for bitumen with n-alkanes heavier than n-C_4 were obtained by extrapolating the correlation of Kumar (2016). Detailed description of the characterization of the BIP for water with hydrocarbons with references to pertinent experimental data can be found in Venkatramani and Okuno (2015).

(2015), the BIP for water/C_D is estimated by reducing the BIP calculated from Eq. 1 with a scaling factor (λ) of less than unity. The optimum value of λ has been determined to be 0.70 by matching the x_{wL} data measured for Athabasca bitumen by Amani et al. (2013a, 2013b). The resulting BIP for water with C_D is 0.169. **Table 3** gives the matrix of the pair-specific BIPs. **Table 4** shows good agreement between the measured x_{wL} for water/Athabasca bitumen mixtures (Amani et al. 2013a, 2013b) and the predicted x_{wL} with the PR EOS with 0.169 for the BIP for water with C_D.

The phase behavior is reflected in the simulations with STARS, in terms of component K values, defined as the ratio of concentration in one phase to another, tabulated as functions of temperature and pressure. The K values used in the simulations with STARS are independent of composition.

For the base case, K values of water corresponding to V-W equilibrium are calculated with Raoult's law. K values for hydrocarbon components are calculated by use of the PR EOS for a fixed overall composition. For SAGD, the fixed overall composition is 100 mol% live bitumen; for ES-SAGD, the fixed overall composition is 20 mol% solvent and 80 mol% live bitumen.

P (bar)	T (K)	x_{wL} (data)	x_{wL} (EOS)
60.42	548.20	0.5412	0.5064
87.18	573.10	0.6321	0.6321
100.25	583.20	0.6699	0.6877
114.50	593.10	0.7192	0.7464
131.00	603.50	0.7477	—
148.30	613.40	0.7964	—
167.20	623.20	0.8274	—
189.90	633.80	0.8462	—
216.47	644.00	0.8620	—

Table 4—Comparison between predicted and measured values of x_{wL} for water-containing Athabasca bitumen. The BIP for water with bitumen (0.169) has been calculated with Eq. 1 scaled by a factor of 0.70. The properties for water and characterized dead Athabasca bitumen (C_D) are shown in Table 2. The pressure/temperature conditions shown in this table are near the L-V-W/L-W boundary. The experimental data were measured for the overall composition of 81.15 mol% water and 18.85 mol% bitumen by Amani et al. (2013b). The "—" indicates a homogeneous liquid phase.

For the water-dissolution case, K values of all components corresponding to L-V-W equilibrium are generated by use of the PR EOS for the fixed overall composition of 90 mol% water and 10 mol% hydrocarbon. For ES-SAGD, the overall distribution of hydrocarbons is set to 2 mol% solvent and 8 mol% live bitumen. This overall composition is representative of conditions near the chamber edge.

To facilitate application in STARS, the L-phase viscosity (μ_L) is modeled as

$$\ln \mu_L = \sum_{i=1}^{N_c} q_i x_{iL} \ln \mu_{iL}, \quad \ldots\ldots\ldots\ldots\ldots\ldots (2)$$

subject to

$$\sum_{i=1}^{N_c} q_i x_{iL} = 1, \quad \ldots\ldots\ldots\ldots\ldots\ldots\ldots (3)$$

where μ_{iL} and x_{iL} are the viscosity and mole fraction of the ith component in the L phase, respectively. q_i is the weighting factor for the ith component, and can be a function of the L-phase composition. C_D is set as the key component in this research; the weighting factors for all nonkey components are set identical to each other. Eq. 2 reduces to the conventional logarithmic mixing model when q_{CD} is set to unity. Composition-dependent functional forms have been developed for q_{CD} on the basis of experimental data for the L-phase viscosity [Glandt and Chapman (1995) for SAGD; Kumar (2016); Nourozieh et al. (2013, 2015a, 2015b) for ES-SAGD].

The composition-dependent function was developed for q_{CD} for SAGD as follows:

$$q_{CD} = a x_{CDL}^6 + b x_{CDL}^5 + c x_{CDL}^4 + d x_{CDL}^3 + e x_{CDL}^2 + f x_{CDL} + g, \quad \ldots\ldots\ldots\ldots\ldots (4)$$

subject to $0 < x_{CDL} < 1$, where $a = -33.95059$, $b = 142.19326$, $c = -242.14374$, $d = 212.01349$; $e = -97.35521$, $f = 19.05086$, and $g = 1.19182$. Note that the L phase consists of the water, methane, and C_D components for SAGD. In the water/C_D binary limit in composition space, use of Eq. 4 in Eq. 2 for SAGD renders the calculated L-viscosity to be approximately equal to that obtained from the linear mixing rule:

$$\mu_L = \sum_{i=1}^{N_c} x_{iL} \mu_{iL}. \quad \ldots\ldots\ldots\ldots\ldots\ldots\ldots (5)$$

The linear mixing rule for the L-phase viscosity was recommended by Glandt and Chapman (1995) for water-containing oil and bitumen.

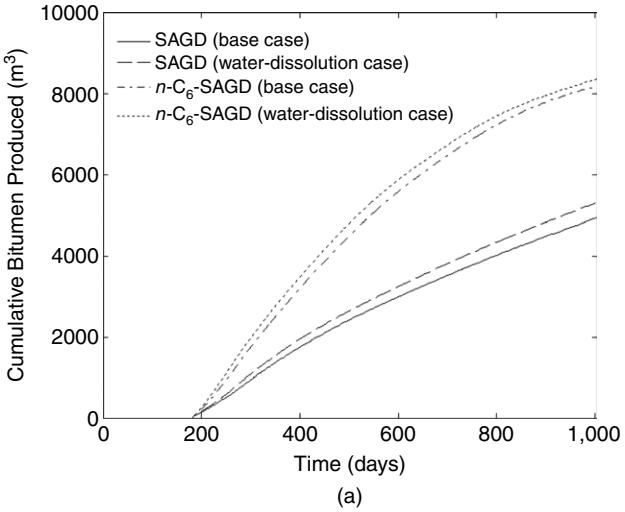

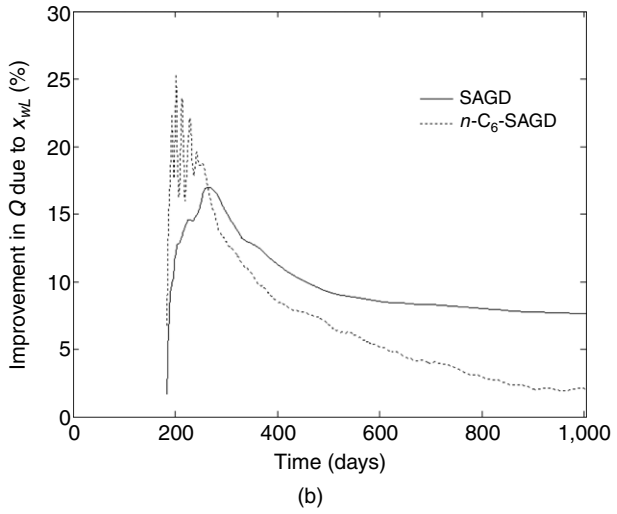

Fig. 1—Effect of x_{wL} on cumulative bitumen production (Q) for SAGD and n-C_6-SAGD: (a) cumulative bitumen-production histories; (b) improvement in cumulative bitumen production caused by x_{wL}. For the water-dissolution case, the steam chamber reaches the outer boundary of the reservoir model at 1,004 days for SAGD and 670 days for n-C_6-SAGD. The original bitumen in place at stock-tank conditions is 11 591 m^3. The linear mixing rule (Eq. 5) is used to model the L-phase viscosity in SAGD. Although the consideration of x_{wL} results in increased estimates for bitumen recovery in both SAGD and n-C_6-SAGD, the extent to which x_{wL} improves bitumen production in SAGD is greater than that for n-C_6-SAGD. This occurs because of higher operating temperatures for SAGD than for n-C_6-SAGD, which results in greater x_{wL} (also see Figs. 2 and 3).

For ES-SAGD, the L phase consists of the water, methane, solvent, and C_D components. The following equation is used for q_{CD}:

$$q_{CD} = 1 + \alpha(\mathrm{CN})\left\{\frac{(1-x_{CDL})[1-(1-x_{CDL})^8]}{x_{CDL}}\right\}, \quad \ldots \quad (6)$$

where α is a parameter specific to the n-alkane solvent under consideration. The optimum α values exhibit a monotonically decreasing trend with respect to the n-alkane carbon number (CN); that is, transition toward the logarithmic mixing rule is observed as the n-alkane CN increases. The values for the α parameter used in the simulations are 0.5498 for C_3, 0.4273 for n-C_4, 0.3562 for n-C_5, 0.3050 for n-C_6, 0.2219 for n-C_7, 0.1464 for n-C_8, 0.0709 for n-C_9, and 0.0 for n-C_{10}. The development of the L-phase viscosity model is described in Appendix A. The choice of mathematical formulation for q_{CD} dictates the type of mixing rule. From a quantitative standpoint, there is uncertainty

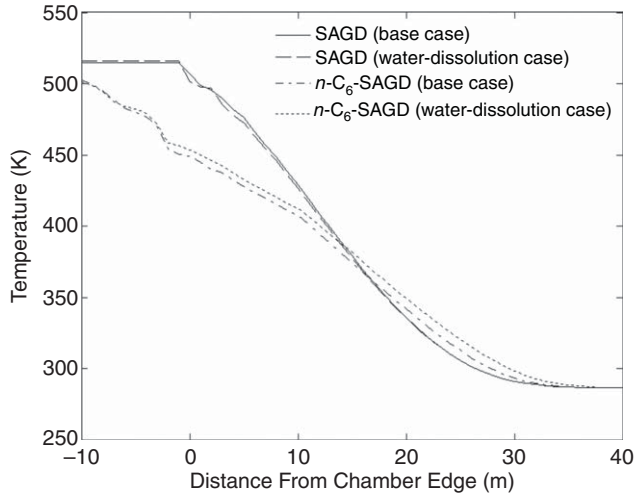

Fig. 2—Temperature profiles for the 12th row (grid layer) from the top of the reservoir model at 578 days from the start of the operation for the base and water-dissolution cases.

in the viscosity models used in this paper, which arises from the scarcity of reliable experimental data for the L-phase viscosity. This uncertainty is discussed further in the Sensitivity Analysis subsection and Appendix A.

The volumetric behavior of the L phase is modeled by a mixing rule that is linear in terms of component-specific molar volumes (i.e., no volume change on mixing),

$$\underline{V}_L = \sum_{i=1}^{N_c} x_{iL}\underline{V}_{iL}, \quad \ldots \quad (7)$$

where $\underline{V}_L$ is the molar volume of the L phase and $\underline{V}_{iL}$ is the molar volume of the ith component in the L phase. A discussion on the applicability of the linear mixing rule for the L-phase molar volume is given in Appendix B.

Analysis of Simulation Results. This subsection consists of two parts. In the subsection Effect of x_{wL} on SAGD and ES-SAGD, the effects of x_{wL} on SAGD and ES-SAGD are investigated. In the Sensitivity Analysis subsection, a sensitivity analysis is conducted to examine the influence of choice of mixing model for the L-phase viscosity, operating pressure, and injection concentration of solvent on the extent to which x_{wL} affects bitumen production.

Effect of x_{wL} on SAGD and ES-SAGD. The operating pressure is set to 35 bar unless stated otherwise. For the simulations for ES-SAGD, the concentration of the solvent in the injection stream is set to 2 mol%, unless otherwise stated.

The consideration of x_{wL} results in improved bitumen production for both SAGD and ES-SAGD. The mechanism for the improvement in bitumen production is the enhancement of the L-phase mobility caused by x_{wL}. After the stabilization of the chamber-edge temperature, which is approximately 365 days from the start of the operation, the average improvement in cumulative production caused by x_{wL} is higher for SAGD than for ES-SAGD. **Fig. 1** presents the cumulative bitumen-production histories for the base and water-dissolution cases for SAGD and n-C_6-SAGD. For the water-dissolution case, the steam chamber reaches the outer boundary of the reservoir model at 1,004 days and 670 days from the start of the operation for SAGD and n-C_6-SAGD processes, respectively. Fig. 1b presents the improvement in cumulative bitumen production caused by the consideration of x_{wL} for SAGD and n-C_6-SAGD. When the steam chamber reaches the outer boundary, the improvement in bitumen production caused by x_{wL} is 7.66% for SAGD and 4.08% for n-C_6-SAGD. At earlier times, this difference can be even higher than 15% (Fig. 1b).

The basis for the aforementioned observation can be understood with the aid of temperature and L-phase composition profiles. For each process and both the base and water-dissolution cases, **Figs. 2 and 3,** respectively, present the profiles for

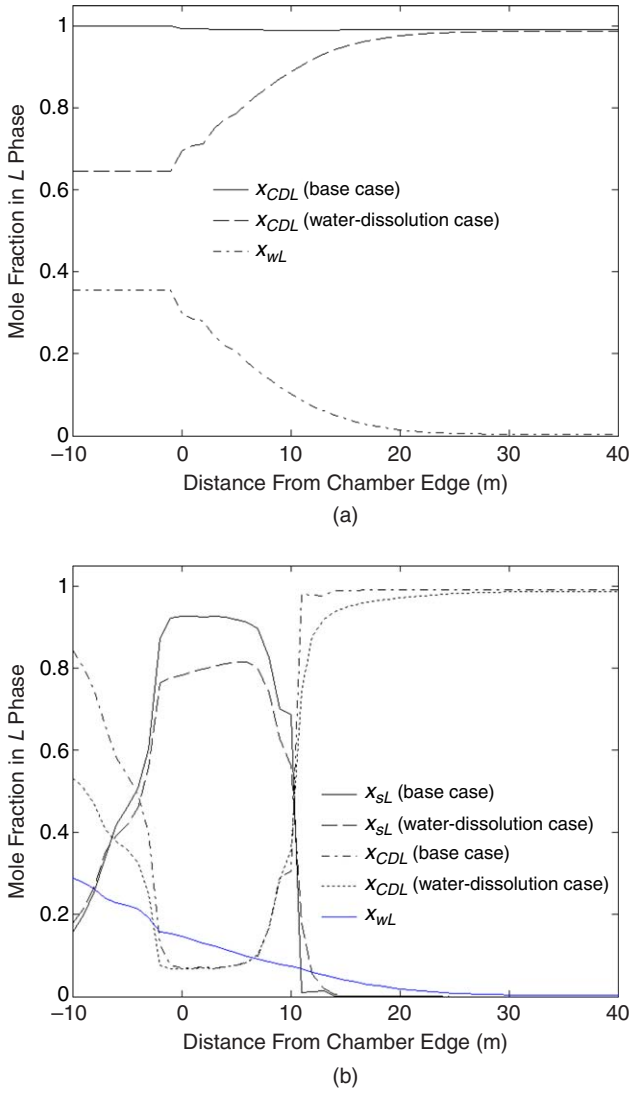

Fig. 3—*L*-phase composition profiles for the 12th row from the top of the reservoir model at 578 days from the start of the operation for the base and water-dissolution cases: (a) SAGD; (b) *n*-C_6-SAGD. When x_{wL} is disregarded in SAGD, the mole fraction of dead bitumen (C_D) in the *L* phase (x_{CDL}) beyond the chamber edge is practically constant at nearly 99 mol%, the initial value used for x_{CDL} in the simulation cases. Consideration of x_{wL} in SAGD results in the monotonic increase of x_{CDL} toward 99 mol% with increasing distance from the chamber edge; this occurs because of the monotonic decrease of x_{wL} with distance, which, in turn, is the result of the monotonic decrease in temperature with increasing distance from chamber edge. When solvent is coinjected (Fig. b), a solvent-rich liquid bank is formed immediately beyond the chamber edge, within which the concentration of the solvent in the *L* phase (x_{sL}) can be substantially greater than x_{CDL}. In this simulation case, consideration of x_{wL} in ES-SAGD results in the lowering of x_{sL}, without significant change in x_{CDL}. The implication here is that the extent to which x_{wL} enhances bitumen production in ES-SAGD for a given solvent depends on the extent to which x_{sL} is lowered because of the dissolution of water in the *L* phase, and the viscosity of the solvent relative to water over the range of temperatures occurring within the solvent-rich liquid bank.

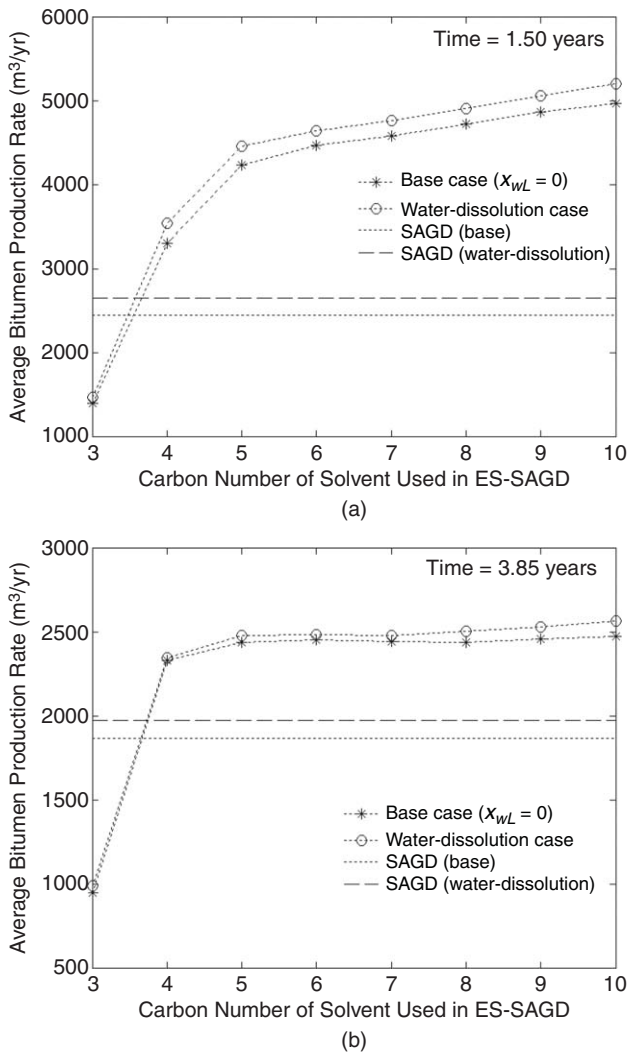

Fig. 4—Average yearly bitumen-production rate for SAGD and ES-SAGD on the basis of cumulative bitumen production at different stages in the production phase: (a) 1.50 years; (b) 3.85 years. In (b), the average bitumen-production rate shows a breakover point at CN 6.

temperature and *L*-phase composition for the 12th row from the top of the reservoir model at 578 days. For a given operating pressure, the effect of x_{wL} on bitumen production is observed to be greater for SAGD because of greater dissolution of water in the *L* phase near the chamber edge. This occurs because of two reasons. First, the temperatures at and in the vicinity of the chamber edge are higher for SAGD than for *n*-C_6-SAGD. Second, the aromaticity of the *L* phase is greater for SAGD in comparison with *n*-C_6-SAGD. The aromaticity of the *L* phase is lowered for *n*-C_6-SAGD because of dissolution of the *n*-alkane solvent in the *L* phase.

For steam-only injection, Luo and Barrufet (2005) have reported an improvement of up to 7% in oil production when x_{wL} is considered. The simulations performed by Luo and Barrufet were for steamflooding and cyclic-steam stimulation. The linear mixing model was used to calculate the *L*-phase viscosity. The maximum temperature in their cases was 505.37 K, which is comparable to the saturation temperature of water at 35 bar (515.72 K); i.e., the injection temperature for the simulations in this section. Despite the greater aromaticity of the bitumen, Fig. 1b indicates that the observed improvement in cumulative bitumen production caused by x_{wL} for SAGD is only slightly higher than the upper bound for the improvement in oil production caused by x_{wL} observed by Luo and Barrufet. It is not clear in their paper how accurately x_{wL} was modeled in their simulations.

The magnitude of improvement in the bitumen production rate caused by consideration of x_{wL} is affected by the volatility of the solvent under consideration. This is apparent from **Fig. 4,** which presents the variation of the yearly average bitumen-production rate with respect to the CN of the solvent at two different times in the production phase (1.50 and 3.85 years). The average bitumen-production rate is calculated on the basis of the cumulative bitumen-production history.

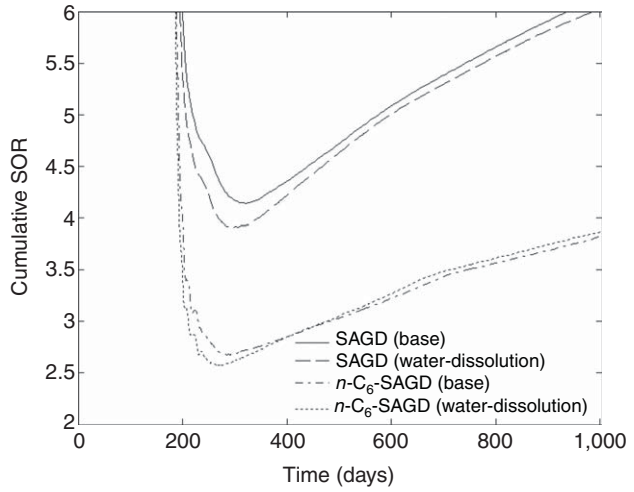

Fig. 5—Effect of x_{wL} on cumulative SOR for SAGD and n-C_6-SAGD at 35 bar. The improvement in the cumulative SOR caused by the consideration of x_{wL} mainly comes from the effect of x_{wL} on cumulative bitumen production. The temperature distribution along and beyond the chamber edge is not significantly affected by accounting for x_{wL}.

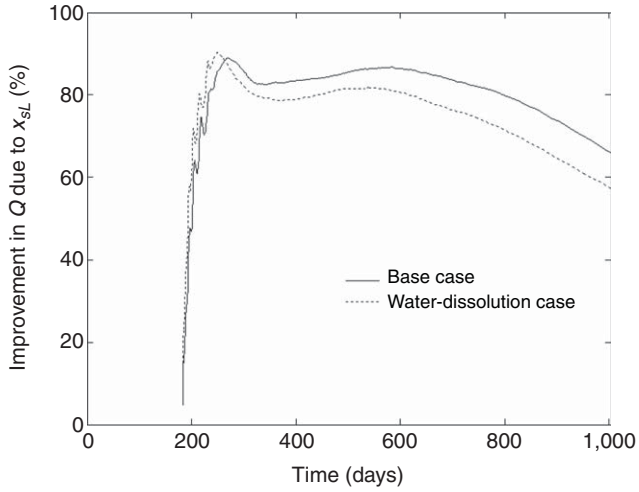

Fig. 6—Relative deviation of n-C_6-SAGD to SAGD in cumulative production of bitumen (Q). Following the stabilization of the chamber-edge temperature, the relative performance of n-C_6-SAGD to SAGD is overestimated when x_{wL} is not considered. For n-C_6-SAGD, the chamber reaches the outer boundary of the reservoir model for the water-dissolution case at 670 days from the start of the operation. At this time, the improvement in bitumen production caused by solvent injection is overestimated by 7.25% (absolute deviation).

The significance of x_{wL} on bitumen-production rate is observed to be higher for heavier solvents (e.g., CNs 8 through 10). This is mainly caused by the combination of higher values for x_{wL} and lower values for the solvent concentration in the L phase (x_{sL}) near the chamber edge, and diminishing capacity of solvent to dilute bitumen compared with water. Consideration of x_{wL} results in lower values for x_{sL} near the chamber edge (see Fig. 3b). The extent of decrease in x_{sL} caused by x_{wL} is a function of temperature. Heavier solvents yield greater values for the chamber-edge temperature and hence, higher temperatures near the chamber edge. This, in turn, results in higher values for x_{wL} and lower values for x_{sL} near the chamber edge. N-alkanes lighter than n-C_9 are less viscous than water; the viscosity of n-C_8 is comparable to that of water at elevated temperatures.

The mechanistic understanding of the effect of x_{wL} on the steam–oil ratio (SOR) is essential because the SOR is an important metric to evaluate the economic feasibility of steam-injection processes. For specified injection strategy, lower values for the cumulative SOR are obtained by increasing bitumen production while lowering heat losses to the formation. When x_{wL} is accounted for, the temperature distribution along and beyond the chamber edge is not significantly altered, as seen in Fig. 2. Hence, its influence on heat losses to the formation is small. Therefore, the extent to which x_{wL} affects the cumulative SOR is limited to its effect on cumulative bitumen production. As cumulative bitumen production is enhanced because of x_{wL}, the resulting cumulative SOR is lower when x_{wL} is considered. **Fig. 5** compares the cumulative SOR histories for the base and water-dissolution cases for SAGD and n-C_6-SAGD. The extent to which the cumulative SOR is reduced for SAGD is higher. This is because the improvement in cumulative bitumen production caused by x_{wL} is greater for SAGD in comparison with ES-SAGD (see Fig. 1).

The simulations indicate that the optimal solvent volatility for the ES-SAGD studied here is between 5 and 7 in terms of the n-alkane CN. The consideration of x_{wL} apparently does not affect this conclusion on the basis of the cases tested here.

The drainage rate of bitumen at and beyond the chamber edge is strongly dependent on the temperature distribution along and beyond it. For a given process, away from the ceiling of the steam chamber, the temperatures along the chamber edge are in the neighborhood of the three-phase temperature of the water/solvent binary corresponding to the operating pressure. This indicates that the temperature distribution near the chamber edge is largely governed by water/solvent phase behavior. Experimental measurements conducted on the phase behavior of water/n-alkane mixtures show that the three-phase temperature corresponding to the transition from L-V-W to L-W equilibrium increases with decreasing volatility of the solvent for specified pertinent pressure of the system (Brunner 1990).

Average bitumen production rates increase monotonically with decreasing solvent volatility early in the production phase, as seen in Fig. 4a. This is mainly because of higher temperatures near the chamber edge, which results in improved viscosity reduction of the L phase and consequently, enhanced L-phase mobility.

Later in the production phase (approximately 3.85 years), a breakover point for the average bitumen-production rate in terms of the solvent volatility is observed to occur in the neighborhood of more volatile solvents (i.e., for CN < 8). This is apparent in Fig. 4b, which presents the variation in average bitumen-production rate with respect to solvent volatility at 3.85 years from the start of production. At this time, the average bitumen-production rates for CNs 5, 6, and 7, respectively are 2442.70, 2453.50, and 2445.30 m^3/year for the base case, and 2482.60, 2486.60, and 2483.20 m^3/year for the water-dissolution case. Occurrence of this break-over point is the result of a balance between temperature and dilution capability of the solvent (Keshavarz et al. 2015). The breakover point occurs near the CN-value of 6 regardless of whether x_{wL} is considered in Fig. 4b.

SAGD serves as the basis upon which the performance of ES-SAGD is evaluated. The simulations conducted thus far show that, with the exception of C_3, the coinjection of solvent with steam yields greater bitumen production compared with steam-only injection. However, the effect of coinjection of solvent with steam is overestimated when x_{wL} is disregarded. This is because the extent to which x_{wL} improves bitumen production in SAGD is greater than that corresponding to ES-SAGD. **Fig. 6** compares the histories of the deviation in cumulative bitumen production for n-C_6-SAGD relative to SAGD for both the base and water-dissolution cases. For n-C_6-SAGD, the chamber reaches the outer boundary of the reservoir model at 670 days when x_{wL} is considered. At this time, the improvement in cumulative bitumen production caused by solvent coinjection for the base and water-dissolution cases is 84.76 and 77.51%, respectively; this represents an overestimation by 7.25%. Fig. 6 suggests that evaluation of production performance of ES-SAGD relative to SAGD be conducted with consideration of x_{wL}; its consideration becomes even more important for evaluations performed at higher operating pressures.

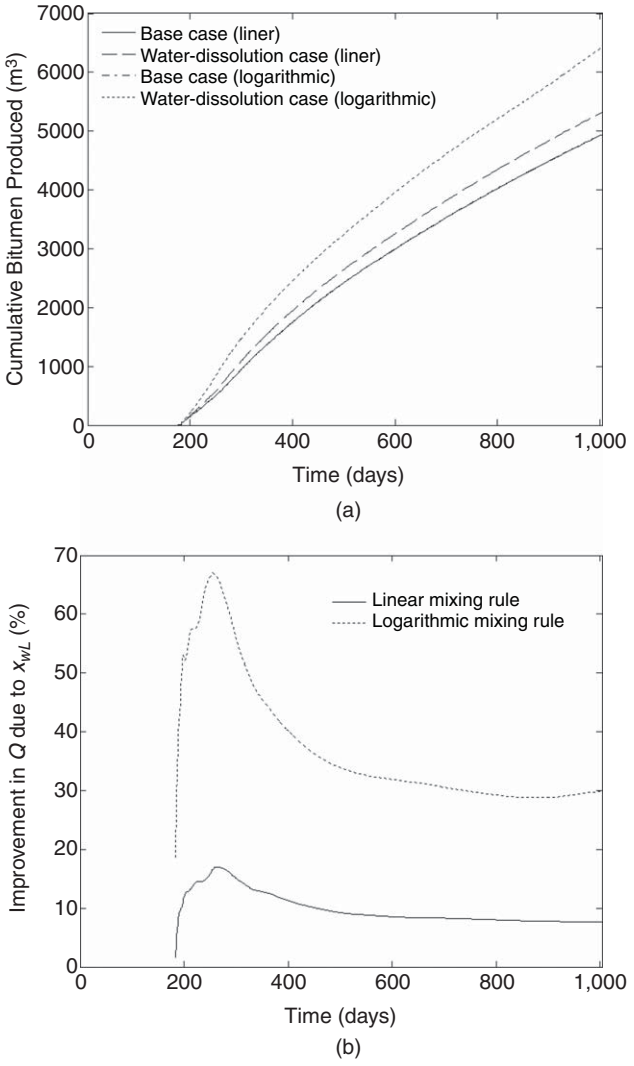

Fig. 7—Effect of the choice of the mixing rule used for the *L*-phase viscosity on SAGD simulation considering x_{wL}: (a) cumulative-bitumen-production histories; (b) improvement in cumulative bitumen production (Q) caused by consideration of x_{wL}.

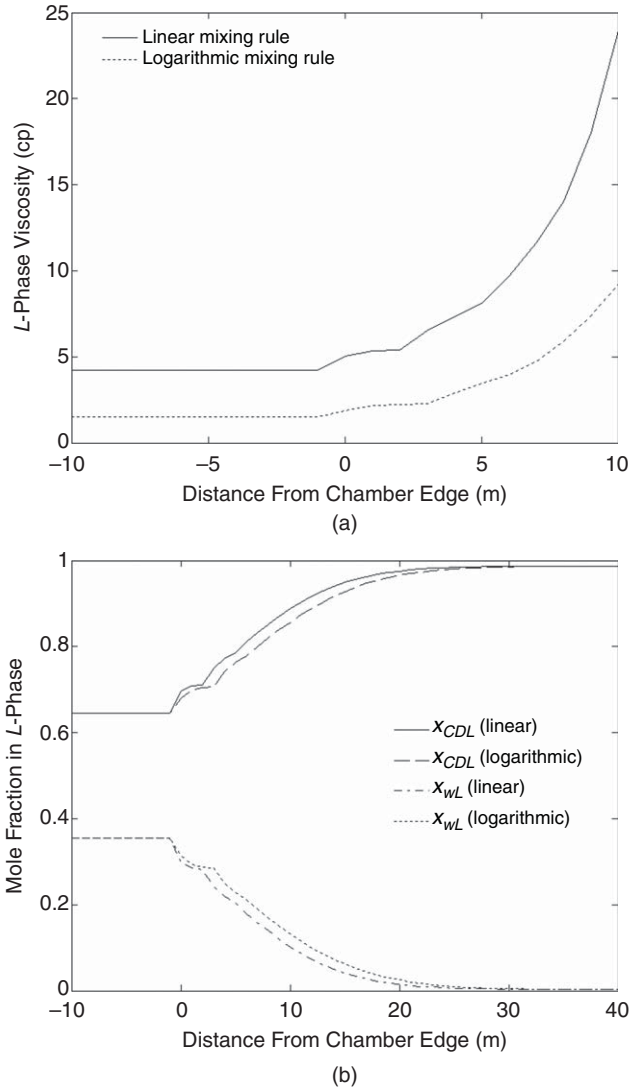

Fig. 8—Effect of *L*-phase viscosity mixing model on property profiles for the water-dissolution case for the 12th row from the top at 578 days from the start of the SAGD operation: (a) *L*-phase viscosity profiles; (b) *L*-phase composition profiles. From (b), it is apparent that the resulting simulated *L*-phase composition profiles from the two models are similar. That is, the extent to which the *L*-phase viscosity is reduced because of a given diluent may be restricted only to the effect that the choice of mixing model has on the weighting factors (q_i) of the components (see Eq. 2).

Sensitivity Analysis. For a given operating pressure, the magnitude of simulated improvement in bitumen production caused by x_{wL} can also be affected by the choice of the mixing model used for the *L*-phase viscosity. **Fig. 7** compares the cumulative bitumen-production histories for the base and water-dissolution cases for the SAGD process for the linear and logarithmic mixing models for the *L*-phase viscosity. As mentioned previously, q_{CD} is assigned the value of unity for the logarithmic mixing rule. The linear mixing rule is given in Eq. 5, and can be approximated with Eq. 4 for q_{CD}. **Fig. 8a** compares the predicted *L*-phase viscosities with the two mixing models for the 12th row from the reservoir top at 578 days from the start of the operation. Fig. 8b presents the pertinent distributions for x_{wL} in the vicinity of the chamber edge.

When x_{wL} is considered, use of the logarithmic mixing rule for the *L*-phase viscosity results in considerably higher improvement in cumulative bitumen production compared with the linear mixing rule (Fig. 7). The main reason for the difference given in Fig. 7 is that, for a specified temperature and *L*-phase composition, the predicted *L*-phase viscosity with the logarithmic mixing rule is considerably lower than that calculated with the linear mixing rule (Fig. 8a). This is because the weighting factor for water (q_w) for a given *L*-phase composition is lower than unity in the linear mixing model (see Eqs. 2 and 3); hence, the contribution of water in lowering the *L*-phase viscosity is diminished under the linear mixing rule. The discrepancy in the simulated x_{wL} profiles for the two mixing models is small, as demonstrated in Fig. 8b.

In the current viscosity-modeling framework, the functional form used for q_{CD} determines the type of mixing model (also see Appendix A). The reliability of the viscosity model is limited by the availability and accuracy of experimental *L*-phase viscosity data because the choice of the mathematical formulation for q_{CD} is informed on the basis of experimental data. This currently is a significant limitation in view of the reliance on numerical simulations for the design and optimization of SAGD and ES-SAGD, the scarcity of reliable experimental data for the *L*-phase viscosity (as described in Appendix A), and the considerable impact that the choice of mixing model for the *L*-phase viscosity can have on bitumen-recovery predictions.

The choice of operating pressure also affects the extent to which x_{wL} enhances bitumen production. **Fig. 9** demonstrates this for the SAGD process. Higher operating pressures result in higher temperatures at and beyond the chamber edge, which results in higher values for x_{wL}, thereby enhancing its contribution to diluting the *L* phase.

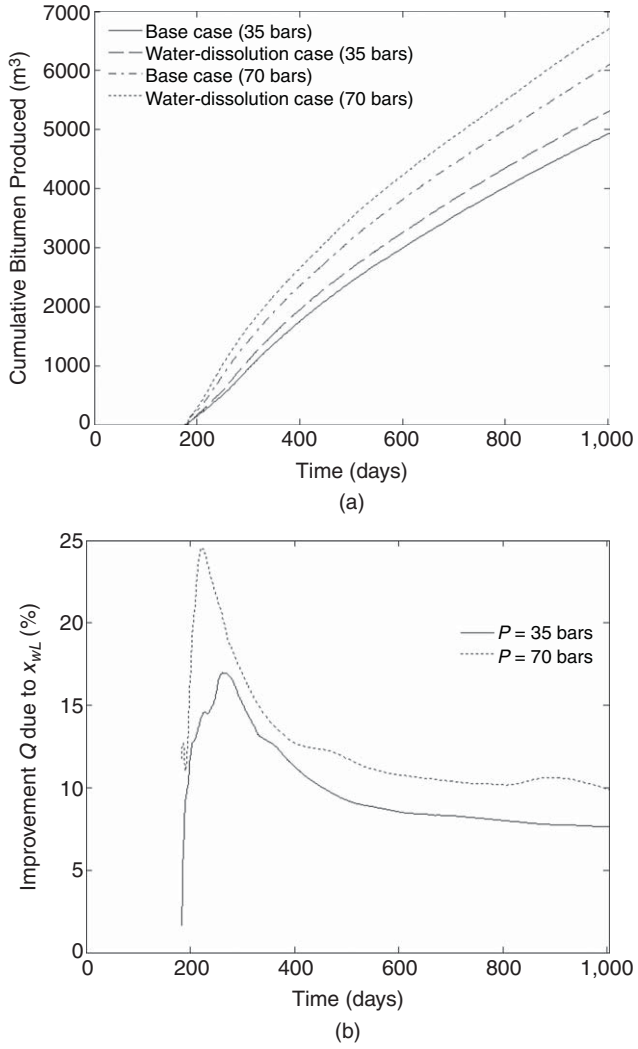

Fig. 9—Effect of operating pressure on magnitude of improvement in cumulative bitumen production caused by x_{wL} in SAGD: (a) cumulative-bitumen-production histories; (b) magnitude of improvement in cumulative bitumen production caused by consideration of x_{wL}. Operating temperatures increase as the operating pressure increases; this enhances x_{wL} and, therefore, the extent to which bitumen production is enhanced because of x_{wL}.

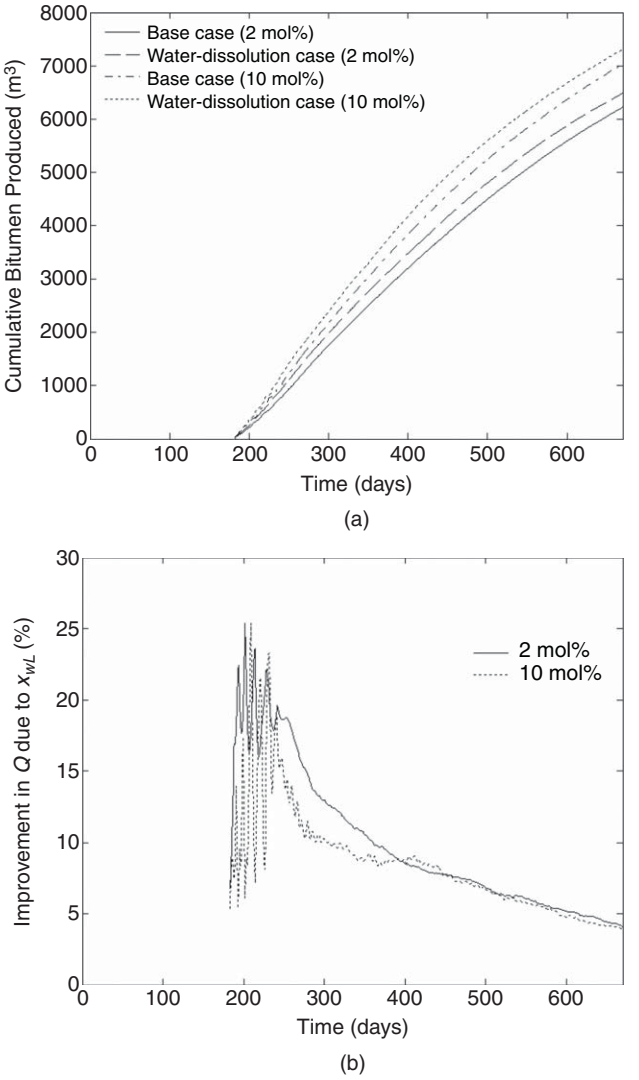

Fig. 10—Effect of injection concentration on magnitude of improvement in cumulative bitumen production caused by x_{wL} in n-C_6-SAGD: (a) 2 mol%; (b) 10 mol%. For the water-dissolution case, the chamber reaches the outer boundary of the reservoir model at 670 days for the 2 mol% case, and 639 days for the 10 mol% case. The extent to which x_{wL} enhances bitumen production reduces because the injection concentration of the solvent increases because of the combined effects of greater dissolution of solvent in the *L* phase within the solvent-rich liquid bank near the chamber edge and occurrence of higher temperatures within the solvent-rich bank. The *L* phase in the high-temperature region within the solvent-rich liquid bank beyond the chamber edge (where x_{wL} is significant) becomes richer in solvent as the injection concentration of solvent increases. This, in turn, diminishes the contribution of the dilution effect brought forth by water toward the drainage rate of bitumen.

For the ES-SAGD process, the choice of the injection concentration can also affect the magnitude of improvement in bitumen production caused by x_{wL} for specified operating pressure. **Fig. 10** compares the cumulative-bitumen-production histories for n-C_6-SAGD corresponding to injection concentrations of 2 mol% and 10 mol%. The steam chamber reaches the right boundary of the reservoir model at 670 days for the 2 mol% case, and 639 days for the 10 mol% case. The improvement in bitumen production caused by x_{wL} is observed to be lower at higher injection concentrations especially at early times in the production phase following the stabilization of the chamber-edge temperature.

The effect of high injection concentrations of solvent on temperature distribution ahead of the chamber edge is small. Thus, the discrepancy in the distribution of x_{wL} ahead of the chamber edge is observed to be small. However, the accumulation of the solvent near the chamber edge is enhanced at higher injection concentrations, which can result in greater solvent dissolution in the *L* phase. This, in turn, diminishes the extent to which water dilutes bitumen.

The most-important conclusion presented in the Effect of x_{wL} on SAGD and ES-SAGD subsection is that the benefit of solvent coinjection in terms of bitumen production can be overestimated when x_{wL} is disregarded. Although not shown in detail in this paper, additional case studies have shown that this conclusion is not significantly affected by a moderate increase in the GOR from 0.44 to 5 m^3/m^3, small to moderate perturbations (2–6%) in the *L*-phase density for hydrocarbons, and an increase in the dimension of the simulations from two to three dimensions.

Injection Strategy for ES-SAGD With Consideration of x_{wL}

The previous section presented a few important results pertaining to the ES-SAGD processes with single-component *n*-alkane solvents on the basis of reservoir simulations. First, ES-SAGD with single-component *n*-alkane solvents with CNs of 4 and higher yielded higher production rates in comparison with SAGD. Second, x_{wL} enhanced bitumen production. Third, the magnitude of

improvement in bitumen production caused by x_{wL} was higher for SAGD relative to ES-SAGD for a specified operating pressure, and increased as the operating pressure was increased for a given process. In this section, a new injection strategy for the ES-SAGD process with *n*-hexane as the solvent is tested to see if it uses x_{wL} to improve bitumen production.

The simulation case studies considered henceforth account for the lateral expansion of the steam chamber on both sides of the well pair. The reservoir is of dimensions $142\,\text{m} \times 500\,\text{m} \times 20\,\text{m}$. The model has been discretized into $71 \times 1 \times 20$ gridblocks in the *x*-, *y*-, and *z*-directions, respectively. As before, the *y*-coordinate in this model represents the direction of the horizontal wells. The scale of the model is increased to obtain a better representation of cumulative bitumen-production histories at the well-pair scale used in field scenarios. The original bitumen in place at stock-tank conditions in these simulation case studies is $313\,520\,\text{m}^3$. The injection and production wells are in the 36th gridblock relative to the left boundary of the model. The production well is subject to a maximum liquid-production rate of $1400\,\text{m}^3/\text{d}$ at surface conditions, which is close to values observed in some field cases. Further, production is carried out under steam-trap control with a minimum subcool of 10 °C.

All simulation case studies presented in this section account for x_{wL} to ensure reliable evaluation of ES-SAGD relative to SAGD. Three injection strategies are considered for ES-SAGD.

In the first strategy, the injection concentrations of the solvent and operating pressure are set to 2 mol% and 35 bar, respectively, during the entire course of the production phase. This is labeled as "CC-CP," where "CC" and "CP" stand for constant concentration and constant pressure, respectively.

The second injection strategy uses a time-variant injection-concentration scheme with the operating pressure held constant. This strategy is labeled as VC-CP, where "VC" denotes variable injection concentration. Its consideration is informed by the observations of Keshavarz et al. (2015). They demonstrated that the injection of solvent at high concentrations early in the production phase expedites the accumulation of the solvent near the chamber edge. This facilitates the enhancement of the production rate of bitumen because of the increased utilization of the dilution capability of solvent. The injection concentration is gradually reduced with time to mitigate solvent retention in the reservoir.

The third injection strategy, which is tested with consideration of x_{wL} for the first time, uses a time-variant operating-pressure scheme alongside a time-variant injection-concentration scheme. This injection strategy is labeled as VC-VP, where "VP" stands for variable pressure.

The consideration of VC-VP is based on the results presented in the previous section. That is, for both the CC-CP and VC-CP strategies, x_{wL} serves as the main mechanism for the dilution of the *L* phase before significant accumulation of the solvent near the chamber edge. As seen in the Mechanistic Study of SAGD and ES-SAGD With Consideration of x_{wL} section, the extent to which x_{wL} dilutes the *L* phase is enhanced with an increase in operating pressure because it results in higher operating temperatures. Hence, the operation of ES-SAGD at elevated pressures early in the production stage is one way to improve the production performance of the VC-CP strategy. This VC-VP strategy is consistent with common practice in SAGD operations, in which operating pressure is higher for the initial stage of production than for the later stages (Jiang et al. 2009).

The performance of ES-SAGD with each of the injection strategies is also compared with that of SAGD using two different injection strategies—"CP," wherein the injection pressure is held constant at 35 bar; and "VP," in which a time-variant injection-pressure scheme is used.

Fig. 11 presents the cumulative-bitumen-production histories for SAGD and ES-SAGD for each injection strategy. The time-variant injection-concentration scheme used for the VC-CP and VC-VP cases shown in Fig. 11 is presented in **Table 5.** As for the time-variant operating pressure scheme for SAGD (VP) and *n*-C_6-SAGD (VC-VP), the operation is carried out at 70 bars for the first two months in the production phase, during which the vertical and lateral expansion of the steam chamber occur simultaneously. After the two months, when the chamber reaches the top of the reservoir model and the lateral expansion of the steam chamber takes precedence, the operating pressure is reduced to 35 bar. For *n*-C_6-SAGD, the steam chamber reaches the outer boundaries of the reservoir model at approximately 912 days from the start of the operation (approximately 24 months into the production phase) for all three injection strategies. For the time-variant injection-concentration strategies, the switch to steam-only injection is made after the steam chamber reaches the outer boundaries of the reservoir model (see Table 2).

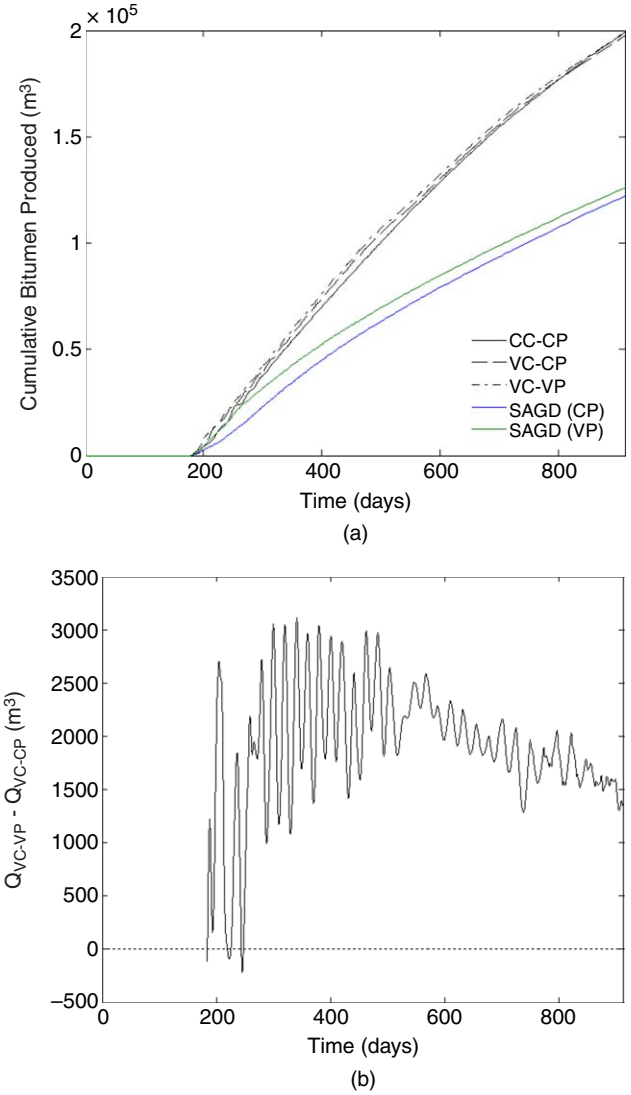

Fig. 11—Bitumen-production performance for SAGD and *n*-C_6-SAGD for the water-dissolution case for different operating scenarios: (a) cumulative-bitumen-production histories; (b) difference between the cumulative bitumen production for VC-VP and VC-CP in ES-SAGD with *n*-C_6 as the solvent. The variation in the injection concentration with respect to time for the VC cases is presented in Table 5. In the VP strategy for both SAGD and *n*-C_6-SAGD, the operation is carried out at 70 bar during the first 2 months of the production phase, and is subsequently reduced to 35 bar. The original bitumen in place at stock-tank conditions is 31 3520 m^3. The linear mixing model (Eq. 5) is used to predict the *L*-phase viscosity in SAGD. In Fig. 11b, the cumulative bitumen production for the VC-CP strategy ($Q_{VC\text{-}CP}$) corresponding to each pertinent time has been subtracted from the corresponding cumulative bitumen production for the VC-VP strategy ($Q_{VC\text{-}VP}$).

Time From Start of Production (months)	Time Including Heating Period (days)	Solvent Concentration (mol%)
0–2	182–244	10
2–10	244–486	5
10–18	486–731	2
18–24	731–912	1
>24	>912	0

Table 5—Time-variant injection-concentration strategy. The reservoir is subject to an initial heating period of 182 days (approximately 6 months) with steam-only injection and no production.

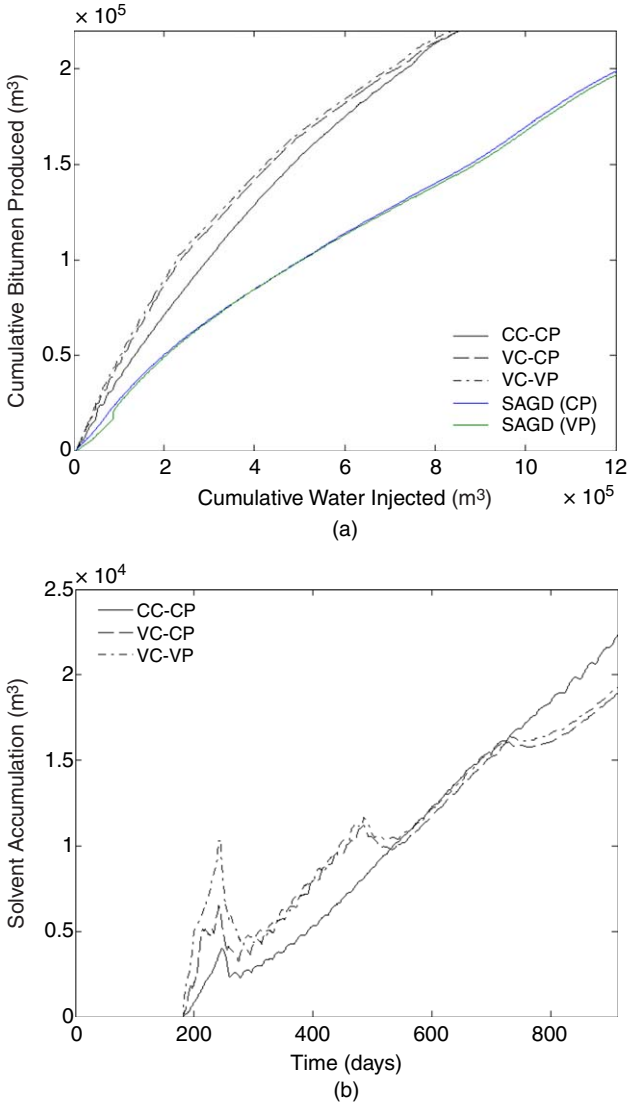

Fig. 12—(a) Steam requirement for SAGD and *n*-C_6-SAGD, and (b) solvent accumulation in *n*-C_6-SAGD for the water-dissolution case for different operating scenarios. In the VP strategy for both SAGD and *n*-C_6-SAGD, the operation is carried out at 70 bar during the first 2 months of the production phase, and is subsequently reduced to 35 bar. In (b), there are three apparent spikes: one near 244 days, the second near 486 days, and the third near 730 days. The first spike corresponds to the transition in the dominant mode of steam-chamber expansion from vertical to lateral, which occurs because of the steam chamber reaching the top of the reservoir model. The other spikes occur because of a change in the injection concentration of the solvent, from 5 to 2 mol% at 486 days, and 2 to 1 mol% at 731 days (also see Table 5).

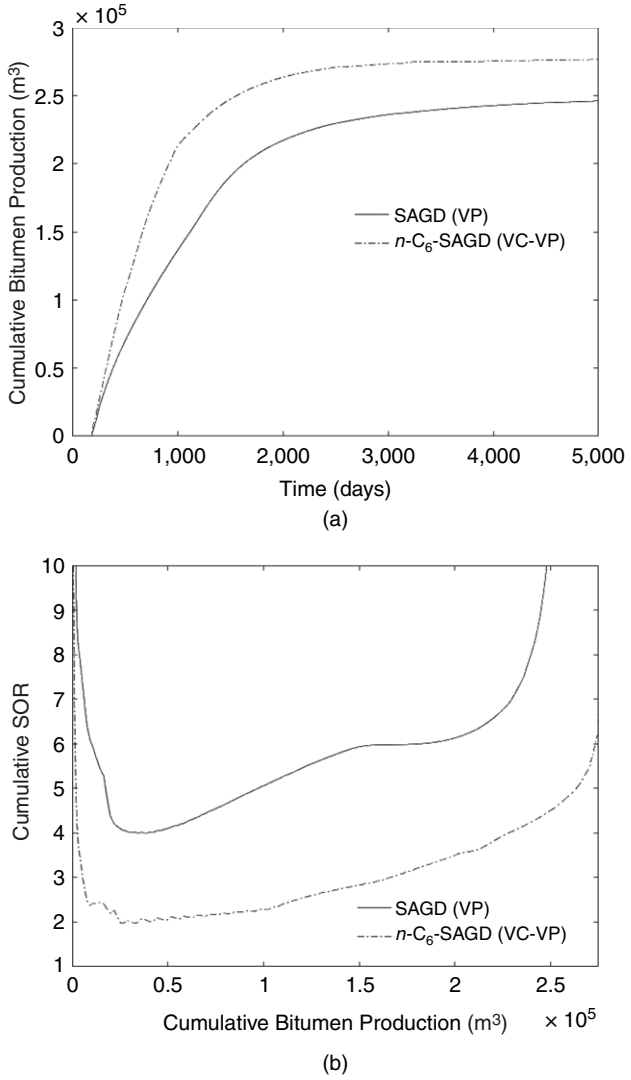

Fig. 13—(a) Cumulative bitumen-production history, and (b) cumulative SOR for SAGD under the VP strategy and *n*-C_6-SAGD under the VC-VP strategy during the long term.

Fig. 11a indicates that, for each process, the implementation of a time-variant operating-pressure scheme (VC-VP for *n*-C_6-SAGD, VP for SAGD) yields the highest cumulative bitumen production during the majority of the duration of the production phase until the chamber reaches the outer boundaries of the model. Fig. 11b shows that the VC-VP strategy can yield 1000 m^3 more production than the VC-CP strategy during the short-term. For SAGD, the corresponding improvement can be in excess of 3000 m^3 because of higher chamber-edge temperatures, as demonstrated in the previous section (see Fig. 2).

The pertinent steam-requirement and solvent-accumulation histories for the different injection strategies are presented in **Fig. 12.** Fig. 12a shows that, for a given process, the consumption of steam [cold water equivalent (CWE)] for a given bitumen production can also be lowered when the time-variant operating-pressure scheme is used. For *n*-C_6-SAGD, the in-situ retention of solvent at later times is considerably lower for both VC-CP and VC-VP strategies than that for the CC-CP case, as seen in Fig. 12b. VC-VP is also advantageous to expedite solvent accumulation in the initial stage of production (see the rapid increase in solvent accumulation right after the beginning of production in Fig. 12b). This is because the solvent injected tends to be accumulated in the *V* phase, instead of condensing into the *L* phase, at initially higher temperatures with VC-VP. For *n*-C_6-SAGD, the combination of greater bitumen production, slightly lower steam

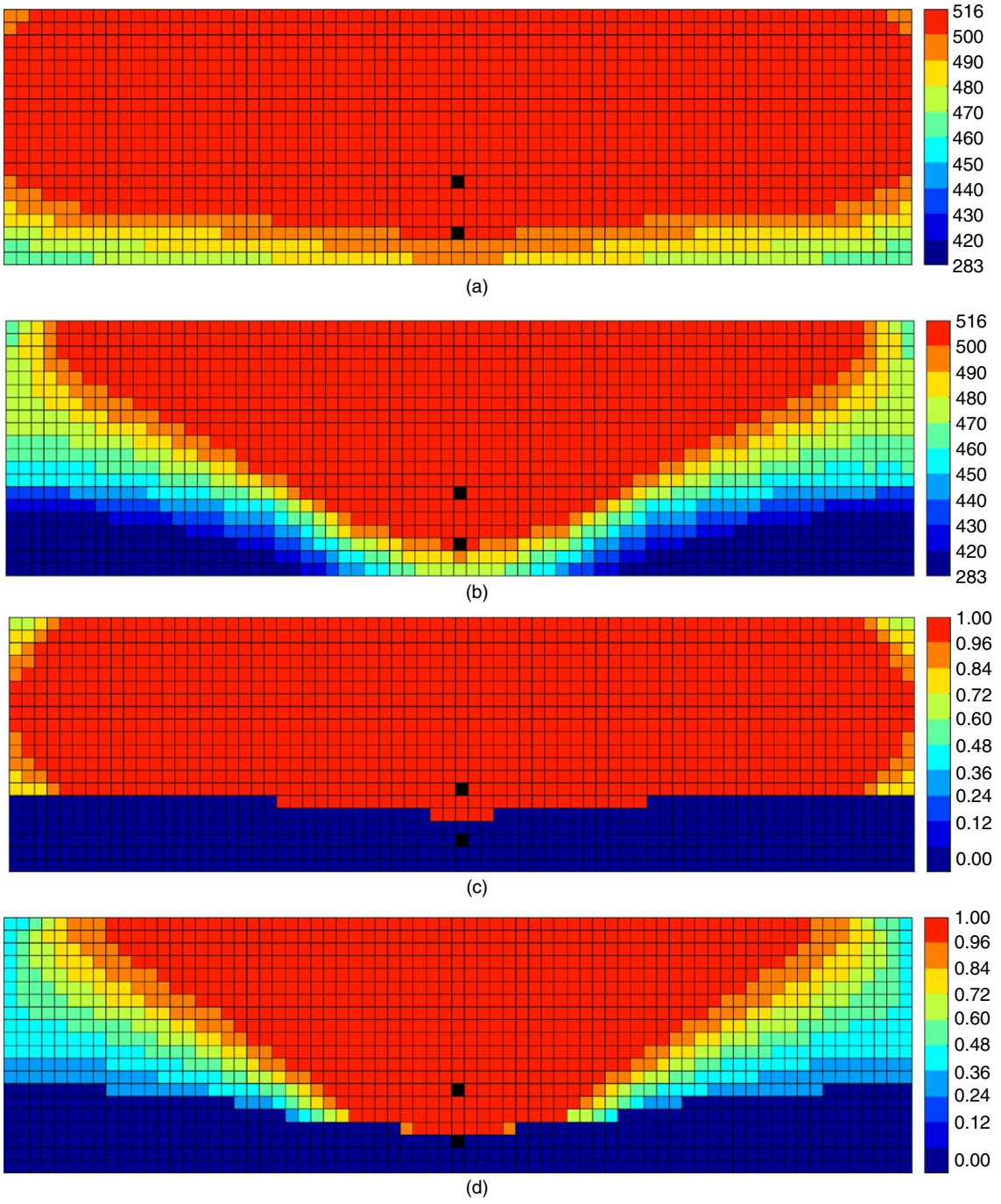

Fig. 14—Maps for temperature (in K) and mole fraction of water in the vapor phase (x_{wV}) for SAGD and *n*-C_6-SAGD corresponding to the cumulative bitumen production of 240 000 m^3: (a) temperature map for SAGD; (b) temperature map for *n*-C_6-SAGD; (c) x_{wV} map for SAGD; and (d) x_{wV} map for *n*-C_6-SAGD. Gridblocks containing the wells are shown in black. The steam chambers in both SAGD and ES-SAGD have reached the outer boundary of the reservoir model in these maps. The coinjection of solvent results in lower temperatures near the periphery of the steam chamber (no-flow boundaries in this example). The injected solvent accumulates in the *V* phase, which makes cooler parts of the steam chamber. The partial condensation of water in the *V* phase results in reduced x_{wV}.

consumption, and comparable solvent accumulation during the majority of the solvent-coinjection period render the VC-VP strategy to be superior to the VC-CP strategy, and hence, the best of the three strategies tested in terms of production performance.

Fig. 13 compares the cumulative bitumen-production histories and accompanying SOR for SAGD under the VP strategy and *n*-C_6-SAGD under the VC-VP strategy during a substantially longer period (≈13 years). The histories for the CP strategies are not shown in Fig. 13 because, for a given process, the ultimate recovery of bitumen is practically identical under both operating-pressure strategies.

Fig. 13a shows that the coinjection of solvent can enhance the ultimate recovery of bitumen in comparison with steam-only injection; this occurs mainly because of the improvement of the local-displacement efficiency within the steam chamber. The improvement in local-displacement efficiency is illustrated with temperature, composition, and saturation maps for a fixed cumulative bitumen production (i.e., a fixed swept region by the steam chamber in these 2D cases). **Fig. 14** presents the maps for temperature and concentration of water in the *V* phase (x_{wV}) for the cumulative bitumen production of 240 000 m^3. **Fig. 15** presents the corresponding *L*-phase saturation maps. The dilution of bitumen by solvent increases the volatility of the *L* phase. Within the steam

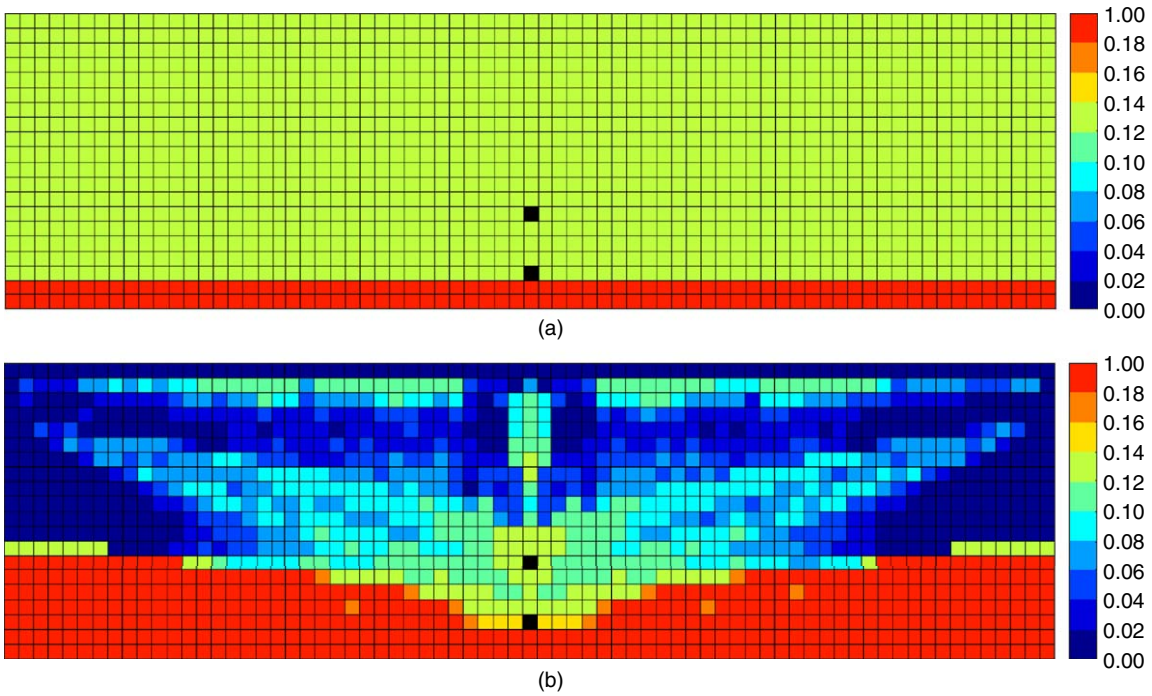

Fig. 15—*L*-phase saturation maps for (a) SAGD and (b) *n*-C_6-SAGD corresponding to the cumulative bitumen production of 240 000 m^3. Gridblocks containing the wells are shown in black. The vaporization of solvent is accompanied by the decrease in the *L*-phase saturation in Fig. 15b. The value of the *L*-phase saturation can be lower than the residual oleic-phase saturation (0.13) used to define the relative permeability curve for the *L* phase. Because of this distillation mechanism, the local displacement efficiency of bitumen can be higher for *n*-C_6-SAGD than for SAGD, which contributes to a higher ultimate recovery of bitumen. The lowest value of the *L*-phase saturation simulated within the steam chamber is 7×10^{-8}.

chamber, continuous injection of steam can vaporize the solvent dissolved in the oleic phase, leading to its accumulation in the V phase. The evaporated solvent accumulates to make cooler regions of the steam chamber, where partial condensation of water occurs. The accumulation of the solvent in the V phase is accompanied by the reduction in x_{wV} (see Fig. 14d). This distillation reduces the L-phase saturation to values lower than the residual L-phase saturation (0.13) used to define the relative permeability of the L phase, resulting in improved local-displacement efficiency of bitumen inside the steam chamber (see Fig. 15b).

Fig. 13b indicates that the cumulative SOR for n-C_6-SAGD can be lower than that for SAGD even at times significantly after the switch to steam-only injection. This is the result of the combination of improved recovery of bitumen and lower heat loss to the overburden and underburden, which is mainly caused by lower operating temperatures. For both the VC-CP and VC-VP strategies, nearly 94% of the injected solvent is simulated to be recovered during a production period of 13 years.

Conclusions

This paper presented a detailed mechanistic study of SAGD and ES-SAGD with consideration of x_{wL} with numerical simulations. Different injection strategies were tested to examine the effect of x_{wL} on the performance of SAGD and ES-SAGD with n-alkane solvents. The phase-behavior model used in the simulations was carefully created on the basis of experimental studies presented in the literature. On the basis of limited experimental data, the L-phase viscosity was modeled such that the dissolution of water in bitumen would lower the L-phase viscosity. Conclusions are as follows:

- Bitumen production was simulated to be improved with consideration of x_{wL} for SAGD and ES-SAGD. For a given operating pressure, the improvement in bitumen production caused by x_{wL} was higher for SAGD than for ES-SAGD. This is because SAGD, in general, yields higher chamber-edge temperatures than ES-SAGD for a given operating pressure. Hence, reliable evaluation of the benefit of solvent coinjection relative to steam-only injection requires the consideration of x_{wL}. This may become more important at higher operating pressures because the temperatures along and beyond the chamber edge increase with increasing operating pressure.
- The magnitude of improvement in bitumen production caused by x_{wL} is sensitive to the mixing model used for the L-phase viscosity. The viscosity model used in this research properly reflects the qualitative difference between the bitumen/water and bitumen/solvent systems that has been reported in the literature. However, it is important to obtain more experimental data for viscosities of bitumen/solvent/water mixtures over a wide temperature range that is relevant to SAGD, to mitigate the uncertainty in the predicted L-phase viscosity from a quantitative standpoint. This would facilitate better understanding of compositional mechanisms in SAGD and ES-SAGD.
- x_{wL} affected the cumulative SOR mainly through the production rate in the simulation cases studied with the STARS simulator. The temperature along and beyond the chamber edge was not significantly affected by x_{wL}.
- The optimal solvent volatility for steam/solvent coinjection for specified operating conditions was not altered when x_{wL} was accounted for in the simulation cases in this research.
- Bitumen-recovery rate in SAGD can be enhanced by using a time-variant operating-pressure strategy (VP). The bitumen-production rate in ES-SAGD can be enhanced by using a time-variant injection concentration and pressure strategy (VC-VP). In SAGD, the VP strategy facilitates increased leveraging of the bitumen dilution by water. In ES-SAGD, the VC-VP strategy additionally expedites solvent accumulation near the chamber edge, although the long-term effect on bitumen production may be small.

Nomenclature

a = coefficient in Eq. 4
b = coefficient in Eq. 4

c = coefficient in Eq. 4
d = coefficient in Eq. 4
e = coefficient in Eq. 4
f = coefficient in Eq. 4
g = coefficient in Eq. 4
L = oleic phase
P = pressure
q = weighting factor for L-phase viscosity
Q = cumulative bitumen production
R = ratio of bitumen price to solvent cost
T = temperature
V = vapor phase
V = molar volume
W = aqueous phase
x = mole fraction
α = coefficient in Eq. 6
λ = scaling factor for BIP
μ = viscosity
ω = acentric factor

Subscripts

C = critical constant
C_D = dead bitumen
hc = hydrocarbon
L = oleic phase
s = solvent
w = water
W = aqueous phase

Abbreviations

API = American Petroleum Institute
BHP = bottomhole pressure
BIP = binary-interaction parameter
CC = constant concentration
CN = carbon number
CP = constant pressure
CWE = cold-water equivalent
EOS = equation of state
ES = expanding solvent
MW = molecular weight
PR = Peng and Robinson
SAGD = steam-assisted gravity drainage
VC = time-variant concentration
VP = time-variant pressure

Acknowledgments

We gratefully acknowledge the financial support from Japan Petroleum Exploration Company Limited and Japan Canada Oil Sands Limited.

References

Abdulagatov, I. M. and Rasulov, S. M. 1996. Viscosity of *n*-Pentane, *n*-Heptane and Their Mixtures Within the Temperature Range From 298 K up to Critical Points at the Saturation Vapor Pressure. *Berichte der Bunsengesellschaft für physikalische Chemie* **100** (2): 148–154. https://doi.org/10.1002/bbpc.19961000211.

Al-Bahlani, A. and Babadagli, T. 2009. SAGD Laboratory Experimental and Numerical Simulation Studies: A Review of Current Status and Future Issues. *Journal of Petroleum Science and Engineering* **68:** 135–150. https://doi.org/10.1016/j.petrol.2009.06.011.

Amani, M. J., Gray, M. R., and Shaw, J. M. 2013a. Phase Behavior of Athabasca Bitumen Water Mixtures at High Temperature and Pressure. *The Journal of Supercritical Fluids* **77:** 142–152. https://doi.org/10.1016/j.supflu.2013.03.007.

Amani, M. J., Gray, M. R., and Shaw, J. M. 2013b. Volume of Mixing and Solubility of Water in Athabasca Bitumen at High Temperature and Pressure. *Fluid Phase Equilibria* **358:** 203–211. https://doi.org/10.1016/j.fluid.2013.07.021.

Brunner, E. 1990. Fluid Mixtures at High Pressures IX. Phase Separation and Critical Phenomena in 23 (*n*-alkane + water) mixtures. *The Journal of Chemical Thermodynamics* **22** (4): 335–353. https://doi.org/10.1016/0021-9614(90)90120-F.

Canadian Association of Petroleum Producers. 2015. *Alberta Oil Sands Bitumen Valuation Methodology*.

Computer Modelling Group. 2011. *STARS Version 2011 User Guide*. Calgary, Alberta, Canada: CMG.

Crabtree, A. and Simon-Tov, M. 1993. *Thermophysical Properties of Saturated Light and Heavy Water for Advanced Neutron Source Applications (No. ORNL/TM-12322)*. Tennessee, USA: Oak Ridge National Laboratory.

Dymond, J. H. and Young, K. J. 1980. Transport Properties of Nonelectrolyte Liquid Mixtures—I. Viscosity Coefficients for *n*-Alkane Mixtures at Saturation Pressure from 283 to 378 K. *International Journal of Thermophysics* **1** (4): 331–344. https://doi.org/10.1007/BF00516562.

Dymond, J. H. and Oye, A. H. 1994. Viscosity of Selected Liquid *n*-Alkanes. *Journal of Physical and Chemical Reference Data* **23** (1): 41–53. https://doi.org/10.1063/1.555943.

Economou, I., Heidman, J., Tsonopoulos, C. et al. 1997. Mutual Solubilities of Hydrocarbons and Water: III. 1-Hexene, 1-Octene, C10- C12 Hydrocarbons. *AIChE Journal* **43** (2): 535–546. https://doi.org/10.1002/aic.690430226.

Glandt, C. A. and Chapman, W. G. 1995. Effect of Water Dissolution on Oil Viscosity. *SPE Res Eng* **10** (1): 59–64. SPE-24631-PA. https://doi.org/10.2118/24631-PA.

Griswold, J. and Kasch, J. E. 1942. Hydrocarbon-Water Solubilities at Elevated Temperatures and Pressures. *Industrial and Engineering Chemistry* **34** (7): 804–806. https://doi.org/10.1021/ie50391a007.

Heidman, J. L., Tsonopoulos, C., Brady, C. J. et al. 1985. High-Temperature Mutual Solubilities of Hydrocarbons and Water. Part II: Ethylbenzene, Ethylcyclohexane, and *n*-Octane. *AIChE Journal* **31** (3): 376–384. https://doi.org/10.1002/aic.690310304.

Heidemann, R. A. 1974. Three-Phase Equilibria Using Equations of State. *AIChE Journal* **20** (5): 847–855. https://doi.org/10.1002/aic.690200504.

Jiang, Q., Thornton, B., Houston, J. R. et al. S. 2009. Review of Thermal Recovery Technologies for the Clearwater and Lower Grand Rapids Formations in the Cold Lake Area in Alberta. Presented at the Canadian International Petroleum Conference, Calgary, 16–18 June. CIPC Paper 2009-068.

Kariznovi, M. 2013. *Phase Behaviour Study and Physical Properties Measurement for Athabasca Bitumen/Solvent Systems Applicable for Thermal and Hybrid Solvent Recovery Processes*. PhD thesis, University of Calgary, Alberta, Canada (October).

Kariznovi, M., Nourozieh, H., and Abedi, J. 2014. Volumetric Properties of Athabasca Bitumen + *n*-Hexane Mixtures. *Energy & Fuels* **28** (12): 7418–7425. https://doi.org/10.1021/ef5019884.

Keshavarz, M., Okuno, R., and Babadagli, T. 2014. Efficient Oil Displacement Near the Chamber Edge in ES-SAGD. *Journal of Petroleum Science and Engineering* **118:** 99–113. https://doi.org/10.1016/j.petrol.2014.04.007.

Keshavarz, M., Okuno, R., and Babadagli, T. 2015. Optimal Application Conditions for Steam/Solvent Coinjection. *SPE Res Eval & Eng* **18** (1): 20–38. SPE-165471-PA. https://doi.org/10.2118/165471-PA.

Khaledi, R., Boone, T. J., Motahhari, H. R. et al. 2015. Optimized Solvent for Solvent Assisted-Steam Assisted Gravity Drainage (SA-SAGD) Recovery Process. Presented at the SPE Heavy Oil Technical Conference, Calgary, 9–11 June. SPE-174429-MS. https://doi.org/10.2118/174429-MS.

Kobayashi, R. and Katz, D. 1953. Vapor-Liquid Equilibria for Binary Hydrocarbon-Water Systems. *Industrial and Engineering Chemistry* **45** (2): 440–446. https://doi.org/10.1021/ie50518a051.

Kumar, A., and Okuno, R. 2015. Direct Perturbation of the Peng-Robinson Attraction and Covolume Parameters for Reservoir Fluid Characterization. *Chemical Engineering Science* **127:** 293–309. https://doi.org/10.1016/j.ces.2015.01.032.

Kumar, A. 2016. *Characterization of Reservoir Fluids Based on Perturbation From n-Alkanes*. PhD thesis, The University of Alberta (January).

Luo, S. and Barrufet, M. A. 2005. Reservoir Simulation Study of Water-in-Oil Solubility Effect on Oil Recovery in Steam Injection Process. *SPE Res Eval & Eng* **8** (6): 528–533. SPE-89407-PA. https://doi.org/10.2118/89407-PA.

Maczynski, A., Shaw, D. G., Goral, M. et al. 2005. IUPAC-NIST Solubility Data Series. 81. Hydrocarbons With Water and Seawater—Revised and Updated. Part 4. C6H14 Hydrocarbons With Water. *Journal of Physical and Chemical Reference Data* **34** (2): 709–753.

Mehrotra, A. K. and Svrcek, W. Y. 1986. Viscosity of Compressed Athabasca Bitumen. *The Canadian Journal of Chemical Engineering* **64:** 844–847. https://doi.org/10.1002/cjce.5450640520.

Nourozieh, H. 2013. *Phase Partitioning and Thermo-physical Properties of Athabasca Bitumen/Solvent Mixtures*. PhD thesis, University of Calgary, Alberta, Canada (September).

Nourozieh, H., Kariznovi, M., Guan, J. G. et al. 2013. Measurement of Thermophysical Properties and Modeling for Pseudo-binary Mixtures of *n*-Decane and Athabasca Bitumen. *Fluid Phase Equilibria* **347:** 62–75. https://doi.org/10.1016/j.fluid.2013.03.010.

Nourozieh, H., Kariznovi, M., and Abedi, J. 2014. Measurement and Prediction of Density for the Mixture of Athabasca Bitumen and Pentane at Temperatures up to 200°C. *Energy & Fuels* **28** (5): 2874–2885. https://doi.org/10.1021/ef4022784.

Nourozieh, H., Kariznovi, M., and Abedi, J. 2015a. Viscosity Measurement and Modeling for Mixtures of Athabasca Bitumen/*n*-Pentane at Temperatures up to 200°C. *SPE J.* **20** (2): 226–238. SPE-170252-PA. https://doi.org/10.2118/170252-PA.

Nourozieh, H., Kariznovi, M., and Abedi, J. 2015b. Viscosity Measurement and Modeling for Mixtures of Athabasca Bitumen/Hexane. *Journal of Petroleum Science and Engineering* **129:** 159–167. https://doi.org/10.1016/j.petrol.2015.03.002.

Oliveira, M. B., Coutinho, J. A. P., and Queimada, A. J. 2007. Mutual Solubilities of Hydrocarbons and Water With the CPA EoS. *Fluid Phase Equilibria* **258** (1): 58–66. https://doi.org/10.1016/j.fluid.2007.05.023.

Peng, D. Y. and Robinson, D. B. 1976. A New Two-Constant Equation of State. *Industrial and Engineering Chemistry Fundamentals* **15** (1): 59–64. https://doi.org/10.1021/i160057a011.

Reamer, H. H., Olds, R. H., Sage, B. H. et al. 1944. Phase Equilibria in Hydrocarbon Systems. *n*-Butane–Water System in Three-Phase Region. *Industrial and Engineering Chemistry* **36** (4): 282–284. https://doi.org/10.1021/ie50411a022.

Robinson, D. B and Peng, D. Y. 1978. The Characterization of the Heptanes and Heavier Fractions for the GPA Peng-Robinson Programs. Gas Processors Association Research Report RR-28.

Shaw, D. G., Maczynski, A., Goral, M. et al. 2005. IUPAC-NIST Solubility Data Series. 81. Hydrocarbons With Water and Seawater—Revised and Updated. Part 7. C8H12–C8H18 Hydrocarbons With Water. *Journal of Physical and Chemical Reference Data* **34** (4): 2261–2298.

Shaw, D. G., Maczynski, A., Goral, M. et al. 2006a. IUPAC-NIST Solubility Data Series. 81. Hydrocarbons With Water and Seawater-Revised and Updated. Part 9. C10 Hydrocarbons With Water. *Journal of Physical and Chemical Reference Data* **35** (1): 93–151.

Shaw, D. G., Maczynski, A., Goral, M. et al. 2006b. IUPAC-NIST Solubility Data Series. 81. Hydrocarbons With Water and Seawater-Revised and Updated. Part 11. C13–C36 Hydrocarbons With Water. *Journal of Physical and Chemical Reference Data* **35** (2): 687–784.

Shinta, A. A. and Firoozabadi, A. 1997. Predicting Phase Behavior of Water/Reservoir-Crude Systems With the Association Concept. *SPE Res Eng* **12** (2): 131–137.

Skripka, V. G. 1979. Solubility of Water in Normal Alkanes at Elevated Temperatures and Pressures. *Chemistry and Technology of Fuels and Oils* **15** (2): 88–90. https://doi.org/10.1007/BF00749406.

Tsonopoulos, C. and Wilson, G. M. 1983. High-Temperature Mutual Solubilities of Hydrocarbons and Water. Part I: Benzene, Cyclohexane and *n*-Hexane. *AIChE Journal* **29** (6): 990–999. https://doi.org/10.1002/aic.690290618.

Tsonopoulos, C. 1999. Thermodynamic Analysis of the Mutual Solubilities of Normal Alkanes and Water. *Fluid Phase Equilibria* **156** (1): 21–33. https://doi.org/10.1016/S0378-3812(99)00021-7.

Venkatramani, A. and Okuno, R. 2015. Characterization of Water Containing Oil Using an EOS for Steam Injection Processes. *Journal of Natural Gas Science and Engineering* **26:** 1091–1106. https://doi.org/10.1016/j.jngse.2015.07.036.

Wagner, W. and Pruß, A. 2002. The IAPWS Formulation 1995 for the Thermodynamic Properties of Ordinary Water Substance for General and Scientific Use. *Journal of Physical and Chemical Reference Data* **31** (2): 387–535. https://doi.org/10.1063/1.1461829.

Younglove, B. A. and Ely, J. F. 1987. Thermophysical Properties of Fluids. II. Methane, Ethane, Propane, Isobutane, and Normal Butane. *Journal of Physical and Chemical Reference Data* **16** (4): 577–798. https://doi.org/10.1063/1.555785.

Zirrahi, M., Hassanzadeh, H., and Abedi, J. 2015. Prediction of Water Solubility in Petroleum Fractions and Heavy Crudes Using Cubic-Plus-Association Equation of State (CPA-EoS). *Fuel* **159:** 894–899. https://doi.org/10.1016/j.fuel.2015.07.058.

Appendix A: *L*-phase Viscosity Model for Water/Solvent/Bitumen

The viscosity of C_D at different temperatures in the vicinity of 35 bar, the operating pressure of the simulation case studies, is given in **Table A-1.** The viscosities of *n*-alkanes and water in the *L* phase correspond to that in the saturated liquid state. The pertinent component-specific viscosity data can be found in Dymond and Young (1980), Younglove and Ely (1987), Crabtree and Simon-Tov (1993), Dymond and Oye (1994), and Abdulagtov and Rasulov (1996). For several of the solvents considered in the study, the temperatures in the interior of the steam chamber away from the edge can be in excess of the critical temperature of the solvent. At these temperatures, the liquid-phase viscosities of the solvent are obtained by extrapolation of the saturated liquid-viscosity curve of the solvent.

Composition-dependent functions for q_{CD} are developed by matching experimental data; the development is restricted by data availability. However, *L*-phase viscosity data are available only for two pseudobinaries, which are water/bitumen and solvent/bitumen.

Simulations for ES-SAGD in this research use the q_{CD} functions developed with *L*-phase viscosity measurements for the solvent/bitumen binary. *L*-phase viscosity data for *n*-alkane/Athabasca-bitumen mixtures are available for *n*-alkanes with CNs 3, 4, 5, 6, and 10 (Nourozieh et al. 2013, 2015a, 2015b; Kumar 2016).

T (K)	μ_{CDL} (cp)	T (K)	μ_{CDL} (cp)
283.150	2457801.750	413.150	42.300
293.150	479830.640	423.150	31.000
303.150	114116.110	433.150	23.500
313.150	32282.500	443.150	18.300
323.150	10642.800	453.150	15.010
333.150	4072.870	463.150	12.500
343.150	1650.000	473.150	10.640
353.150	787.000	483.150	9.240
363.150	422.000	493.150	8.160
373.150	241.000	503.150	7.310
383.150	133.000	513.150	6.640
393.150	85.600	523.150	6.100
403.150	58.700		

Table A-1—Viscosity data for dead Athabasca bitumen at different temperatures. These data have been measured near 35 bar, the operating pressure for most of the simulation case studies used in this work.

CN	α	Data Points	Temperature (K)	ARD (%) (solvent/C_D)	Data Sources	ARD (%) (water/C_D)	AAD (cp) (water/C_D)
3	0.5498	2	373.15	3.42	Kumar (2016)	18.18	1.25
4	0.4273	2	423.15	9.00	Kumar (2016)	30.24	1.96
5	0.3562	18	374.00 – 464.00	33.26	Nourozieh et al. (2015a)	36.30	2.33
6	0.3050	18	374.00 – 464.00	29.78	Nourozieh et al. (2015b)	40.29	2.58
10	0.0000	60	301.00 – 344.00	9.62	Nourozieh et al. (2013)	58.85	3.81

Table A-2—Optimized values for the α-parameter for ES-SAGD cases. The error in the predicted *L*-phase viscosity in the water/bitumen limit has been evaluated against the synthetic data generated for temperatures between 464 K and 558 K. The ARD in this limit is considerably lower between 283 K and 558 K. Although the ARD for *n*-C_5/Athabasca-bitumen and *n*-C_6/Athabasca-bitumen cases seem high, the corresponding AAD values for the predicted *L*-phase viscosities are only 0.92 cp and 1.05 cp, respectively.

Eq. 6 (see the Mechanistic Study of SAGD and ES-SAGD With Consideration of x_{wL} section) gives the general functional form for q_{CD} developed on the basis of the experimental data where the α parameter is specific to the *n*-alkane solvent under consideration. The second term on the right-hand side of Eq. 6 may be viewed as a function that represents the departure from the logarithmic mixing rule.

The optimum α values exhibit a monotonically decreasing trend with respect to the *n*-alkane CN. That is, transition toward the logarithmic mixing rule is observed as the *n*-alkane CN increases. The pertinent values for the α parameter are presented in **Table A-2.** Because of the limited data availability, the α values for *n*-alkanes with CNs 7 through 9 have been determined with a linear fit shown next:

$$\alpha(\mathrm{CN}) = -0.07551\mathrm{CN} + 0.75051. \quad \ldots\ldots\ldots\ldots \text{(A-1)}$$

Eq. A-1 gives the R^2 value of 0.9618 for the set of optimized values for the α parameter with respect to the *n*-alkane CN. When Eq. 6 is used in the water/bitumen limit, systematic underestimation of the *L*-phase viscosity is observed. Nevertheless, Eq. 6 is preferable for application in ES-SAGD simulations. This is because the alternative approach, which is the use of Eq. 4, is considerably more erroneous when applied in the solvent/bitumen limit.

For SAGD simulations, a composition-dependent function for q_{CD} has been developed on the basis of data corresponding to the water/bitumen edge in composition space. For water/Athabasca-bitumen, *L*-phase viscosity data have not been published, to the best of our knowledge. Therefore, a composition-dependent function for q_{CD} was developed with synthetic data.

The synthetic data were generated on the basis of the experimental study conducted by Glandt and Chapman (1995) on the *L*-phase viscosity of water-containing Peace River bitumen. The temperatures in these experiments lie between 434 and 558 K. The corresponding experimental pressures are near the boundary between two and three phases where the aqueous phase (*W*) can exist (Personal communication with W. G. Chapman, Rice University, Houston). For water-containing Peace River bitumen, Glandt and Chapman (1995) have demonstrated that the conventional logarithmic mixing rule overestimates the reduction of the *L*-phase viscosity caused by x_{wL}. On the other hand, the linear mixing rule, given in Eq. 5 (see Mechanistic Study of SAGD and ES-SAGD With Consideration of x_{wL} section), was shown to satisfactorily predict the *L*-phase viscosity over the aforementioned temperature range.

Synthetic *L*-phase viscosity data for water/Athabasca bitumen have been generated with a two-step process. For temperatures between 434 and 558 K, and pressures slightly higher than the corresponding saturation pressure of water, the composition of the *L* phase is first determined by performing *P-T* flash calculations. The linear mixing rule is subsequently applied to calculate the *L*-phase viscosity. The composition-dependent function developed for q_{CD} with the synthetic data is presented in Eq. 4 in the Mechanistic Study of SAGD and ES-SAGD With Consideration of x_{wL} section. Use of Eq. 4 results in the average relative deviation (ARD) and absolute average deviation (AAD) values of 0.17% and 0.12 cp, respectively, with respect to the synthetic *L*-phase viscosity data generated between 434 and 558 K.

Appendix B: *L*-phase Density Model for Water/Solvent/Bitumen

The numerical simulations in this paper use the linear mixing rule for the *L*-phase molar volume (Eq. 7). This appendix discusses the implementation of the linear mixing rule in STARS and its applicability in reservoir simulation. In terms of the mass density, Eq. 7 can be rewritten as

$$\rho_L = \mathrm{MW}_L\left[\sum_{i=1}^{N_C}\left(x_{iL}\mathrm{MW}_i/\rho_{iL}\right)\right]^{-1}, \quad \ldots\ldots\ldots\ldots \text{(B-1)}$$

where MW_L is the molecular weight of the *L* phase; MW_i is the molecular weight of the *i*th component; and ρ_L and ρ_{iL} are the mass density of the *L* phase and the *i*th component in the *L* phase, respectively.

To facilitate application in STARS (CMG 2011), the component-specific mass densities (ρ_{iL}) in the *L* phase are correlated with the following functional form:

$$\rho_{iL} = \rho_{i\mathrm{ref}} e^{a_1(p-p_{\mathrm{ref}}) - a_2(T-T_{\mathrm{ref}}) - 0.5a_3(T^2-T_{\mathrm{ref}}^2) + a_4(p-p_{\mathrm{ref}})(T-T_{\mathrm{ref}})}, \quad \ldots\ldots\ldots\ldots \text{(B-2)}$$

where $T_{\mathrm{ref}} = 288.15$ K and $P_{\mathrm{ref}} = 101.325$ kPa (= 1.01325 bar). $\rho_{i\mathrm{ref}}$ corresponds to the density of the *i*th component at T_{ref} and P_{ref}. For the calculation of the mass density at an arbitrary *P-T* condition with Eq. B-2, the pertinent units to be used are kPa for pressure and K for temperature. The values of a_1 through a_4 for each component are determined by optimization against measured data. For *n*-alkanes and bitumen, these coefficients have been obtained from Kumar (2016).

The pertinent coefficients for water have been determined by optimization against the saturated liquid-phase density data calculated with the experimentally determined correlation recommended by Wagner and Pruß (2002),

$$\rho_{wL} = 0.322\left(1 + b_1\vartheta^{\frac{1}{3}} + b_2\vartheta^{\frac{2}{3}} + b_3\vartheta^{\frac{5}{3}} + b_4\vartheta^{\frac{16}{3}} + b_5\vartheta^{\frac{43}{3}} + b_6\vartheta^{\frac{110}{3}}\right), \quad \ldots\ldots\ldots\ldots \text{(B-3)}$$

where $\vartheta = 1 - (\mathrm{T}/647.096)$; $b_1 = 1.99274064$; $b_2 = 1.099653042$; $b_3 = -0.510839303$; $b_4 = -1.75493479$; $b_5 = -45.5170352$; and $b_6 = -6.74694450 \times 10^5$.

Between 283.15 and 558.15 K, the ARD resulting from use of Eq. B-3 is 0.16%. The values for ρ_{iref} and coefficients a_1 through a_4 for different water/solvent/Athabasca-bitumen mixtures are given in **Tables B-1 and B-2.**

Component	ρ_{ref} (kg/m^3)	a_1	a_2	a_3	a_4
Water	998.5	0.00E+00	–1.67E–03	6.48E–06	0.00E+00
C_1	320.15	5.13E–06	1.32E–03	5.77E–06	4.05E–08
C_3	651.83	3.02E–06	2.12E–04	5.46E–06	1.08E–08
n-C_4	769.81	2.55E–06	5.19E–05	5.05E–06	4.56E–09
n-C_5	823.47	2.20E–06	–8.87E–05	4.77E–06	2.88E–09
n-C_6	858.69	1.88E–06	–1.21E–04	4.20E–06	2.04E–09
n-C_7	846.36	1.66E–06	–1.30E–04	3.79E–06	1.59E–09
n-C_8	859.85	1.48E–06	–1.28E–04	3.39E–06	1.23E–09
n-C_9	869.99	1.34E–06	–1.24E–04	3.09E–06	9.84E–10
n-C_{10}	869.99	1.22E–06	–1.17E–04	2.80E–06	7.75E–10

Table B-1—Coefficients for component-specific densities in the *L* phase to be used with Eq. B-2.

System	ρ_{ref} (kg/m^3)	a_1	a_2	a_3	a_4
Water/C_3/C_D	992.64	3.88E–07	–2.23E–05	9.09E–07	3.73E–09
Water/*n*-C_4/C_D	992.64	3.88E–07	–2.23E–05	9.09E–07	4.28E–09
Water/*n*-C_5/C_D	992.64	3.85E–07	–1.95E–05	8.95E–07	4.72E–09
Water/*n*-C_6/C_D	992.64	3.85E–07	–1.93E–05	8.95E–07	4.80E–09
Water/*n*-C_7/C_D	992.64	3.85E–07	–1.95E–05	8.96E–07	4.80E–09
Water/*n*-C_8/C_D	992.64	3.85E–07	–1.98E–05	8.97E–07	4.79E–09
Water/*n*-C_9/C_D	992.64	3.86E–07	–2.01E–05	8.98E–07	4.77E–09
Water/*n*-C_{10}/C_D	992.64	3.86E–07	–2.03E–05	8.99E–07	4.78E–09

Table B-2—Coefficients for density of C_D in the *L* phase to be used with Eq. B-2.

System	Data Points	Data Sources	Temperature (K)	Pressure (bar)	AAD (g/cm^3)	ARD (%)
n-C_5/bitumen	30	Nourozieh et al. (2014)	295–463	39–41	0.065	8.39
n-C_6/bitumen	30	Kariznovi et al. (2014)	296–463	39–41	0.066	8.23
n-C_{10}/bitumen	60	Nourozieh et al. (2013)	296–333	30–40	0.046	5.27
Water/bitumen	21	Amani et al. (2013b)	594–643	54–260	0.045	5.85

Table B-3—Accuracy of the linear mixing rule for prediction of the *L*-phase density of solvent/bitumen and water/bitumen mixtures. For solvent/bitumen mixtures, the validation is performed for pressures in the neighborhood of 35 bar (±5 bar), which is the operating pressure for the simulation cases. The densities of the individual components are calculated with Eq. B-2 with the coefficients presented in Tables B-1 and B-2.

For both water/Athabasca bitumen, and solvent/Athabasca bitumen with *n*-alkane CNs between 5 and 10, use of linear mixing rule to predict the *L*-phase density results in a reasonably good match with respect to the measured data. The pertinent AAD and ARD values are summarized in **Table B-3.**

Arun Venkat Venkatramani is a PhD degree candidate in petroleum engineering at the University of Alberta. His research interests include thermodynamics and transport phenomena. Venkatramani holds BS and MS degrees in chemical engineering from the National Institute of Technology, India, and Arizona State University, respectively, and an MS degree in petroleum engineering from the University of Alberta.

Ryosuke Okuno is an assistant professor in the Department of Petroleum and Geosystems Engineering at The University of Texas at Austin. Before his current position, he served as an assistant professor of petroleum engineering in the Department of Civil and Environmental Engineering at the University of Alberta from 2010 to 2015. Okuno also has 7 years of industrial experience as a reservoir engineer with Japan Petroleum Exploration Company Limited, and is a registered Professional Engineer in Alberta, Canada. His research and teaching interests include enhanced oil recovery, thermal oil recovery, oil-displacement theory, numerical reservoir simulation, thermodynamics, multiphase behavior, and applied mathematics. Okuno is a recipient of the 2012 SPE Petroleum Engineering Junior Faculty Research Initiation Award, is an associate editor for *SPE Journal* and the *Journal of Natural Gas Science & Engineering*, and holds the Pioneer Corporation Faculty Fellowship in Petroleum Engineering at The University of Texas at Austin. He holds BS and MS degrees in geosystem engineering from the University of Tokyo and a PhD degree in petroleum engineering from The University of Texas at Austin.